Frontiers in Health Informatics
ISSN-Online: 2676-7104
www.healthinformaticsjournal.com
2024; Vol 13: Issue 3
Open Access

Metropolitan Metamorphosis: Understanding Urban Expansion and Its Environmental Impacts

[1]Mr. Abhinandan Das,[2]Tapan Kumar Das,[3]Shrutilekha Das

1Department of Humanities and Social Sciences, Indian Institute of Technology Kharagpur, West Bengal 721302, India.
abhinandan94@iitkgp.ac.in, abhinandandas24@gmail.com, abhinandandas2018@gmail.com. Orcid Id: 0000-0003-0660-7770
2Retired Punjab National Bank Staff, Krishnanagar Branch, Krishnanagar, India Independent Researcher.
tapankumardas1000@gmail.com
3Independent Researcher, Barrackpore, India,
shrutilekhadas2020@gmail.com,

Cite this paper as: Abhinandan Das,Tapan Kumar Das,Shrutilekha Das (2024) Metropolitan Metamorphosis: Understanding Urban Expansion and Its Environmental Impacts .*Frontiers in Health Informatics, 13* (3), 3852-3906

Introduction:

An urban area's land use and cover often indicate various anthropocentric and physical two-dimensional land uses. In an urban region, building up residential and commercial sectors takes up the majority of the land. The rapid expansion of urban populations and residential areas has significantly transformed urban regions' LULC. Consequently, several factors combine to determine the extent to which a city's residential, commercial, and transportation regions, as well as its municipal area, population, and the number of settlements, undergo changes in land use and cover within the urban area. Nevertheless, in an urban environment, the factors that exert the most significant influence on the swift growth of the population and residential areas have led to alterations in land utilization and coverage, as well as the replacement of urban land utilization by urban dwellers.

Urban sprawl, often known as urban growth, is the unplanned or unwanted growth of a metropolis into the surrounding rural regions at the expense of the quality of the urban environment. This occurs as a result of factors such as high population pressure, low land prices, improved infrastructure, rising standards of living, a lack of urban planning, lower tax rates, and others. The repercussions of these expansions mostly include altered land uses, the resulting growth in traffic and public infrastructure, health and environmental problems, and altered social dynamics.

Many people have been using GIS and remote sensing to see how cities have grown and changed. They have all demonstrated importance, resilience, efficacy, and precision. Only some studies have used system dynamics models to isolate the factors most responsible for a particular event, even though several simulation and empirical models are available for predicting LULC changes. A practical method for studying LULC at various geographical sizes is to combine the Markov-chain model with cellular automata (CA). These models are powerful tools for conducting quantitative simulations. The cellular automaton (CA) model utilizes a probability matrix to predict spatial transformations within a specific timeframe.

Urban expansion and population growth are signs of a thriving economy. However, the negative impacts of human activities such as deforestation, construction, sewage systems, water supply, transportation networks, and large-scale construction projects on the environment cannot be ignored. These activities have detrimental effects on the land, soil, biodiversity, air, water, and overall environmental well-being. Just like how extensive development turns cities into impermeable surfaces, it also contributes to the formation of heat islands and

exacerbates climate change, leading to more frequent natural disasters.

In conjunction with simulation models, it is imperative to employ RS and GIS techniques to evaluate, track, and replicate previous, current, and forthcoming LULC conditions to tackle these difficulties. By doing this, we can build sustainable development and protect the delicate ecological balance, which could lead to effective urban policies and demographic, economic, and environmental plans. It is essential to gather spatial-temporal characteristics over time to make informed decisions and ensure a harmonious coexistence between urban development and the environment. Agricultural drought monitoring, urban heat island effect, and other fields of research make extensive use of land surface temperature as a key parameter in the movement of matter and energy between the ground and atmosphere. LST is often measured using a thermometer at set observation times and places. Due to the fluctuating fluctuations in LST, this discrete point measuring technique is unable to gather continuous and large-scale LST information. The advancement of satellite thermal infrared remote sensing technology makes it feasible to regularly return huge regions and get the LST distribution.

Microclimates in cities are influenced by the urban heat island effect, which is a significant contributor to urban warming. When city dwellers experience significantly higher air and land surface temperatures than those in more rural locations, this phenomenon is known as the urban heat island effect. Several regional problems, including biophysical dangers like high temperatures, air pollution, and public health concerns, are associated with urban heat islands. To improve city dwellers' health, quality of life, and overall happiness, reducing the warming of urban microclimates by tackling the problem of urban heat islands is essential.

The loss of natural vegetation and water bodies, as well as changes in land use brought about by urbanization, are among the many variables that, according to research, combine to create Urban Heat Island (UHI). Among these factors, urbanization is considered to be the most significant element that leads to alterations in land cover. Changes in land cover, such as replacing vegetation with non-porous surfaces like asphalt, pavement, or roofs, are the primary cause of variations in Land Surface Temperature (LST). Every kind of land cover has unique attributes regarding the release and absorption of energy. Impermeable surfaces, such as those with low albedos, can absorb substantial solar energy. At night, they emit the stored solar energy as thermal infrared heat. Thus, there are differences in Land Surface Temperature (LST) across different land cover types about the day-night cycle. In addition, researchers conducted a cross-sectional analysis to demonstrate a correlation between different forms of land cover and land surface temperature (LST) fluctuations throughout time.

The impact of altering land use and cover on the environment and local climate can be observed during the process of urbanization. One notable effect is the urban heat island (UHI) phenomenon, which occurs when natural areas are converted into impermeable surfaces. This conversion reduces evapotranspiration and increases the absorption and retention of solar radiation in urban areas. As time passes, the intensity of UHI becomes more significant due to the occurrence of extreme heatwave conditions in cities, which can have detrimental health effects such as heat stress and heatstroke. The UHI pattern can be influenced by both external factors like the location and climate conditions of the urban area, as well as internal factors such as land use, land cover, city size and expansion, and human activities. Some of the observed variances in the UHI phenomena can be explained by shifts in underlying causes, the most important of which are the dynamics of LST within cities. The heat from energy use, material changes, and the albedo of pavements and building rooftops are a few factors that might alter the intensity of SUHI over time. Increasing the amount of green space in the urban environment is a well-known method of mitigating the impacts of SUHI.

Rather than utilizing on-site measurements, which offer limited and scattered data, the evaluation of the SUHI phenomenon is frequently conducted using thermal data obtained from satellites. Satellite sensors have the potential to give reliable and constant observations of the Earth's surface, allowing for the examination of urban areas at different geographical and temporal scales. The detailed evaluation of urban heat island (SUHI) variations in a small geographical location is conducted by considering several elements, including land cover, land use, urban site features, landscape composition, and layout. This analysis is integrated into the comprehensive assessment of SUHI utilizing satellite sensors.

Urban planning policy can be effectively regulated by utilizing remote sensing methods and surface ancillary data at various geographical and temporal scales. The SUHI dynamics are often thought of in terms of urban sprawl, changing land use and cover, increased human and industrial activity, and urban materials. However, the impact of seasonality and the daily cycle must be considered by us in dry and semi-arid climates. The changes in SUHI intensity between seasons or years are influenced by both the warming and cooling tendencies of urban and rural regions. It is worth noting that mitigation of SUHI, resulting from a warming trend in rural areas rather than the implementation of urban heat alleviation techniques, may inadvertently lead to an amplification of SUHI, even when there is only a slight increase in urban zone temperatures.

Review of Literature:

Urbanization entails transforming and regulating the natural environment to create an urban setting (Zeng et al., 2019). Urban areas are transforming in terms of their dimensions and compactness due to rapid population expansion (Seto et al., 2012; Reed et al., 2013). By 2030, almost 60% of the global population will reside in urban areas, according to two studies: the 2014 United Nations World Urbanisation Prospects research and the 2019 report by Ghosh et al. Changes to LULC patterns inside cities and the development of urban areas are expected outcomes of fast population growth. Modifying the LULC configuration can adversely affect the environment, impacting vegetation, aquatic ecosystems, grasslands, and undeveloped areas.

LULC changes have become very important to urban planners to control the many environmental issues that come up because of growth (Nuissl et al., 2009).

The natural environment, particularly the urban green cover, is under more stress in many cities, especially in developing countries, because of fast and uncontrolled urban growth (Jenks et al., 2000; Lin et al., 2015).

An increasing number of individuals now concur that climate change has predominantly attributed to land use and land cover (LULC) alterations, which significantly impact biodiversity, biogeochemical cycles, natural processes, and human activities (NRC 1999).

Land use (how people have changed the earth's surface) and land cover (how living things live on the surface) are changing faster because of socioeconomic and biophysical forces (Turner et al. 1995; Lambin et al. 2000). These changes significantly impact the duration of socioeconomic progress as they directly influence crucial components of our natural capital, such as biodiversity, water resources, and vegetation (Mather and Sdasyuk 1991).

Over an extended duration, anthropogenic activities and the natural ecosystem have influenced alterations in land utilization and coverage. It is possible to look at how future changes in land cover might affect the transitions of land using land change modeling (Wang et al., 2021). Several authors have written about how to model future built-up areas using agent-based modeling, knowledge-based expert systems, cellular automata-based algorithms, machine learning-based techniques, and artificial intelligence (Jat et al. 2017).

We can thank the Markov Chain model and the cellular automata (CA) model for their important work. The model utilizes temporal changes from time 't' to time' t + 1' to forecast the probability of land use changes at the future date' t + 1'. The Markov chain is highly effective for estimating Land Use and Land Cover (LULC) based on present patterns. This approach relies on the probability of a specific parcel of land transitioning from two mutually incompatible states (Thomas and Laurence, 2006).

Li and Yeh (2002) showed a new way to model how different land uses have changed over time by combining neural networks with CA in a GIS context. The researchers in this study made a three-layer neural network model with many neurons as output to look at the conversion rates used for competing land uses. Iterative looping is used in neural networks in this model to make the process of land conversion more realistic.

These odds are based on changes that have happened in the past and are used to guess what changes might happen in the future. A random Markov model, on the other hand, isn't good because it doesn't take into account

how spatial knowledge is distributed within each category or how transition probabilities change across landscape states. As a result, it might give the right change's size but not its direction (Boerner et al. 1996).

Ca models were introduced as an option to traditional models in the middle of the 1980s (Torrens and O'Sullivan, 2001). They were simple, could simulate dynamic space, and could make high-resolution models by using GIS and remotely sensed data.

Using Markov chain analysis, Hathout (2002) looked at how urban growth would affect farming land on the edges of urban-rural areas and predicted how fast cities would grow. Maithani (2010) tried to make a model called cellular automata (CA) to help him figure out how cities might grow in the future in India. This model used remote sensing data, real-world data on urban growth, and the Markov chain method to guess how much land will be needed for cities in the future.

These urban simulation models and algorithms are like a sped-up version of a real event. They are used to make up scenarios or situations that show how cities work and change over time (Sangermano et al. 2010). Cellular Automata (CA) models have been used a lot in the last 20 years because they are standard and easy to combine with other spatial research. The CA-Markov model combines the Markov model with the CA-based model to account for interactions between things in the neighborhood. Because it looks at how neighbors interact, it is seen as an important tool for figuring out how the land cover will be spread out in the future (Wang et al., 2021).

Bununu (2017) used a mixed model that combined the Simweight algorithm with the Markov chain model to measure and distribute changes in land use. To describe how things change in the Kansas City Metropolitan area, Zubair et al. (2017) combined a Markov chain model with a machine-learning method called Simweight (similarity-weighted instance).

Mandal et al. (2019) examined land cover and use changes in Kolkata, India, and surrounding areas for nearly 30 years. Various topics were covered in the discussion, including the dynamics of land use and cover, how these change over time and space, the path of urban expansion, regional variations, how to predict future land use and cover using CA-Markov modeling, and methods for estimating population growth.

Geographic Information Systems (GIS) and Remote Sensing (RS) techniques, along with Cellular Automata (CA) and Markov models, are employed to analyze and examine patterns of urban expansion on a global scale. However, not many researchers have used these methods to look at Gandhinagar's urban growth. A mixed model with Markov chains, cellular automata (CA), and a logistic regression model was created to make the classic logistic regression model better at simulating urban growth (Jokar et al., 2013).

It depends on specific groups of laws and rules, which is called land use change. Local raster-based simulations (Shafizadeh and Helbich, 2013; Guan et al., 2011) use discrete time steps to simulate urban growth. GIS may also be beneficial for finding and analyzing changes in land use that are already happening (Celik et al., 2019; Sekertekin et al., 2016).

The CA-Markov model integrates the CA and Markov Chain components to perform many primary assessment tasks. The anticipated modification occurs while employing a transition area matrix, a CA-Markov appeal, and a connectivity kernel to expand land-use maps to a future period utilizing a CA function. According to Pontius et al. (2004a), this can change the Markov Chain's outputs to the desired outcomes. We will examine and document the module's reliability and accuracy. Given the ease of integration with GIS and remote sensing data, a CA-Markov model provides a solid framework for quantifying and describing the spatial and temporal dynamics of LULCC.

The Markov-CA model can be explained, then the chances of transitions can be looked into, and finally, the rules for the area can be shown on future maps using information from biology, society, and the economy (Kamusoko et al. 2009).

Various modeling methods Here, models like the Cellular Automaton (CA) and the Markov Chain have been

used to represent changes in LULC. However, these models still need to prove they can accurately predict the future. Because of this, the CA-Markov model will be used to look at how things have changed in the research area. The research area's land-use maps have been created using Landsat pictures from 2001 to 2021. The goal was to use these maps as a model for making future land-use maps.

The point of this study was to find out how fast, where, and what benefits urban green space (UGS) has on an Indian metropolis that is growing quickly. The literature evaluation unequivocally demonstrates that rapid urban expansion is encroaching upon and causing harm to urban vegetation covering (Li et al., 2016). Urban Green Space (UGS) refers to any vegetated area within an urban environment, including grasslands, trees, parks, home gardens, playgrounds, and other natural places. Supporting biodiversity, lowering air pollution, and reducing the heat island effect are just a few of the many services that UGS makes a big difference in (Dallimer et al., 2016, Zhou et al., 2017, Ferreira and Duarte, 2019, Grigoraş and Uriţescu, 2019). Urban green spaces (UGS) significantly influence the overall quality of residential areas, offering notable advantages for both mental and physical well-being and serving as venues for recreational activities and artistic expression (Taylor and Hochuli, 2017).

Converting green spaces into solid surfaces alters the dynamics of heat transfer, water retention, and the energy equilibrium between the land's surface and the atmosphere in urban areas (Crutzen, 2004). The shift in LST, which leads to the creation of UHI and further deteriorates the health of the environment, is one of the significant repercussions of this land conversion, according to Voogt and Oke (2003), Kaufmann et al. (2007), Sherafati et al. (2018), and Gohain et al. 2021.

In their 2013 paper, Ahmed et al. looked at how land cover changes happen and how they affect LST in Dhaka, Bangladesh. Wang et al. (2016) looked into how cities grow and how that changes LST in Nanjing, China. The study showed that the city has grown quickly by covering up dirt and plants with surfaces that don't let water through. This has caused LST to rise. Guha et al. (2017) used temperature satellite data for Raipur, India, to study how LST is distributed in space and time and how it changes.

Priyankara et al. (2019) looked at how changes in land cover and variations in LST are related in their study of how development affects the growth of UHI. Dissanayake et al. (2019) conducted a study in Kandy City, Sri Lanka, to examine the impact of land use and land cover alterations on the spatial and temporal variations in Land Surface Temperature (LST).

In Pune, Gohain et al. (2021) looked at how LST changed over time and space across different types of land cover. They found that LST and density had grown a lot in built-up areas compared to other types of land cover. In their study, Roy et al. (2020) looked at how changing land cover affected LST and also found that urban heat islands had an impact. The study found that the mean LST went up over urban areas.

In 2020, Jana et al. investigated how the thermal behavior of Doon Valley was affected by the pattern and magnitude of urban expansion. In their study, Das et al. (2021) sought to establish a connection between several spatial indicators by investigating the effects of changing land use and land cover on surface temperature in the Asansol area.

A thorough familiarity with plant anatomy and physiology is necessary to study rainfall patterns and climate change. Regarding crop development and seasonal shifts, NDVI plays a significant role. It has been found that changes in NDVI are related to changes in soil wetness, rainfall, crop production, and natural plant growth. Rainfall and soil wetness have a lot to do with how plants grow and develop (Sharma et al., 2022). Temperature and rainfall have a big effect on how much and what kind of plants grow in an area (Sha et al., 2020).

As cities grow quickly around the world, they change the land's surface in big ways. One of the main things that affects how the LST spread changes is natural vegetation. NDVI is the most popular vegetation index, and it is used to figure out LST. Many things affect the connection between the LST and NDVI, such as the weather, different types of plants, land use, development, and more. Multiple recent studies have focused on finding a

correlation between LST and NDVI in large cities across the globe (Guha and Govil, 2020; Guha, 2021).

To predict the Land Surface Temperature (LST) in the Chinese Taihu Lake Basin, Feng et al. (2018) used three indices. The normalized difference built-up index (NDBI), the normalized difference vegetation index (NDVI), and the normalized difference water index (NDWI) were the indices that were utilized.

Rahman et al. (2017) investigated the impact of land use and cover alterations on land surface temperature (LST). The researchers employed a Cellular Automata Markov (CAM) model to simulate the projected changes in land cover in Dammam, a city on the eastern coast of Saudi Arabia. Additionally, they used a multiple linear regression analysis based on the Modified Normalised Difference Water Body Index (MNDWI) and NDBI to predict the future Land Surface Temperature (LST) in the same area.

There are still a lot of questions about how changes in vegetation affect the climate, especially in Central Asia. However, Yuan et al. (2017) say that changes in vegetation can have a big effect on land surface temperatures in the area.

More people living in cities push the edges of rural areas, which puts stress on them and uses up natural resources like farms, woods, and plants. So, urbanization is a big part of how Land Use and Land Cover (LULC) change, and it's also a good way to guess how LULC will change, which causes surface energy to become uneven and temperatures to rise (Matthews et al., 2015).

Two important climate factors are the combined temperature of the atmosphere in the planetary boundary layer and the temperature of the land's surface (Jin, 1996). The air temperature immediately above the ground's surface is called the "Land Surface Temperature". The temperature was recorded using a shielded thermometer 1.5 to 3.5 meters above a flat, green, unobstructed, and well-ventilated area. Using satellite technology, skin temperature, a distinct form of Land Surface Temperature (LST), can now be employed in any location (Dickinson 1994).

LST is sometimes mistakenly perceived as the temperature in its core. However, the land surface is not a uniform or planar structure; it consists of several heterogeneous materials with diverse shapes, which complicates the determination of land surface tension (Qin and Karnieli 1999). Furthermore, the surface frequently exhibits a significantly uneven topography when using low-resolution satellite measurements. LST can only be accurately defined on uniform surfaces in composition and temperature. Two other names for LST have been proposed in the remote sensing community: surface radiometric temperature (Norman & Becker, 1995) and ensemble directional radiometric surface temperature (Prata et al., 1995).

The variable known as LST holds significant importance in climate and environmental studies. Matsui et al. (Matsui, 2002) say that LST and changes in rainfall during the North American Monsoon are connected. According to Pinheiro et al. (2006), the land's skin temperature can be used to find out things like the surface energy balance, find out if the land's surface has been disturbed, and keep an eye on conditions that make it easy for insect-vector diseases to spread.

Because satellite sensors see the ground surface through different shapes, the zenith angle needs to be taken into account when figuring out the brightness temperatures (Kimes et al. 1980, 1983, Ignatov and Dergileva 1994).

"Ensemble" refers to what a pixel adds to the whole. As well as the measurement's spectral channel for a certain sensor viewing direction, LST is affected by how temperature and emissivity are spread out inside a pixel. It's not limited to surfaces that are uniformly isothermal because it takes into account the effect of the whole "ensemble" inside a pixel. Conversely, the definition of a surface is contingent upon the characteristics of the tools employed to capture the image, such as their dimensions and clarity. It should correspond to the dimensions of the model (Becker and Li 1995).

For this study, Mumtaz et al. (2020) used Landsat data from 1998 to 2018 to look at Peshawar and Lahore, two

very large towns in Pakistan. In Peshawar, there was an increase in both urbanized land and vegetation cover. However, in Lahore, there was just an increase in urbanized land while vegetation cover decreased. Because of this, it has been found that the temperatures in Peshawar and Lahore have been steadily going down and up, respectively.

Despite its significance in regulating LST in urban areas, the number of green spaces in cities worldwide has experienced a substantial decline in the past few decades (Choudhury et al., 2019). The development activities result in significant alterations to the vegetation, leading to a loss of UTE (Xiong et al., 2012). Urban buffers have more significant LST than rural buffers, resulting in the SUHI (Mathew et al., 2018). Urban flash floods, heat waves, higher precipitation, and elevated temperatures are some of the environmental difficulties caused by these events (Santamouris, 2014; Fu & Weng, 2018). Also, ecological concerns and land degradation are present.

In their 2022 study, Waleed and Sajjad examined the impact of urbanization on LST in Pakistan. From 1990 to 2020, the built-up area grew by 8.5% per year, which caused the average maximum LST to rise by 1.4 C. Mathew et al. (2018) used the MODIS dataset to study SUHI in two Indian megacities and found that both cities have a bigger effect on SUHI at night than during the day.

In 2021, Dilawar et al. looked at six major cities in Pakistan's Punjab area to see how urbanization has changed SUHI. The results showed that in all places, vegetation was always going down because more people were moving into the areas, which over time made SUHI worse. The biggest places in South Asian countries were looked at by Hassan et al. in 2021. The author found that more people living in cities are reducing the amount of plant cover in South Asian megacities. Some researchers assert that a 1-2°c temperature difference existed between rural and urban regions.

Various LULC classes contribute to LST differently because of differences in energy absorption and radiative properties, surface reflectance, and roughness (Bokaie et al., 2016; Solaimani et al., 2010). As a result of increased urbanization, several regions have seen a decline in their vegetation cover (Dilawar et al., 2021; Mumtaz et al., 2020; Singh et al., 2017).

The NDVI is a widely utilized and significant remote sensing technique for assessing the vitality of an ecosystem (HanqiuXu, et al., 2019). A higher NDVI shows more vegetation, or the amount or state of vegetation within a pixel. It is common for places with the lowest LSTs to also have the highest NDVI. This negative link between the NDVI and LST is important for studying the climate in cities and the environment (Yuan and Bauer, 2007).

It was found by Weng et al. (2004) that LST and vegetation percent have a weakly negative link. The links between LST and NDVI, on the other hand, change depending on the season and time of day. In winter and warm seasons, there are strong positive and negative links between NDVI and LST. However, Karnieli et al. (2006) show that ecosystems in the north at high latitudes tend to have positive relationships between LST and NDVI.

Aims and Objectives:

1. To evaluate the dynamics of urban growth by analyzing changes in LULC.

2. To examine how changes in land use and land cover affect the spatiotemporal changes in urban green space.

3. To assess metropolitan expansion patterns in the KMDA and analyze the urban expansion collision on surface temperature.

Significance of the Study:

The current effort will aid in the creation of sustainable, smart cities, which is now a priority for the Indian government and will assist urban planning organizations in developing mitigation techniques for urban heat island impacts. Nurwanda and Honjo, 2020; Sekertekin and Zadbagher, 2021; Feng et al. 2018; Rahman et al.

2017; Tran et al. 2017; Feng et al. 2018; and similar investigations are quite a few, and as far as we are aware, no reported attempts have been made in an Indian context. The current study will be conducted in Kolkata city and its surrounding areas (India's West Bengal state).

Study Area:

Kolkata, the capital of West Bengal in India, was originally established by the British. It is situated in a flat region with tide-dominated drainage outfalls. The Kolkata Metropolitan Area (KMA), which includes the city of Kolkata, is one of the world's most important urban areas. KMA, known as The Kolkata Urban Agglomeration (KUA), has experienced consistent growth throughout the past century. KUA spans an area of around 1851 square kilometers and is situated between latitudes 22˚ 0'19''and 23˚0'01'' in the north and 88˚0'04'' and 88˚ 0'33'' in the east. The Hooghly River is a vital lifeline for the entire Southern Bengal region. The city of Kolkata, with its urban sprawl, is situated along both the eastern and western banks of the river, forming a linear urban layout. The rural hinterland envelops the urban area, serving as a buffering green belt around the agglomeration (KMC 2015). This intricate network of local governments in South Bengal includes 38 towns, 77 census towns (CT), 16 expansions, 445 rural villages, and three large municipal corporations (MC): Kolkata, Howrah, and Chandernagore.

With a density of 7950 people per square kilometer, the 2011 Census put the total population of the KMA at approximately 14.72 million. With a projected yearly growth rate of 1.8%, the Indian population is expected to reach 20 million in 2021 and 21.1% in 2025, according to the 2011 Census of India and the KMDA. With a combined population of almost 30 million, the megacities that make up the Kolkata metropolitan agglomeration are among the most populous in the world (UN, 2007). Among India's urban agglomerations, Kolkata ranks third in size. As it grows into a major metropolis, perhaps in comparison to other cities worldwide, Kolkata faces several socioeconomic challenges, including heavy traffic, poverty, overcrowding, noise, water, and air pollution (Bhatta, 2009; Mukherjee, 2012).

On top of that, 33 percent of the people living in the slums of KMA are poor. Multiple land uses, including residential, commercial, and industrial, coexist in the metropolitan agglomeration's slums (Roy et al., 2014; Sugiyama, 2008; Bhatta, 2009). Swamps and marshy areas abound in the easternmost part of the KMA, especially in Bidhan Nagar, Rajarhat, Maheshtala, and Sonarpur. Without adequate planning, these wetland areas are transformed into urban areas by constructing homes (Ghosh & Sen, 1987; Dasgupta et al., 2013).

Methodology:

Therefore, the continuing study primarily aims to assess the impact of land use and land cover changes on the disappearance of urban green areas. The goal is to foretell possible future events by incorporating the CA-Markov model. Additionally, the current study analyses the distribution of green space per capita and the variation in green space availability across cities in terms of space and time. Since NDVI is the principal variable impacting land surface temperature (LST) variations, it is the only variable in this study that deals with discussion on LST. In this study, we analyze the impact of urban land use changes on land surface temperature in the Kolkata Urban Agglomeration utilizing remote sensing and zonal statistic methodologies.

For carrying out this investigation, ground truth information gathered in the field and satellite image data were both employed. The data was systematically compiled and analyzed while keeping the study's goals in mind.

The previous documentation provides detailed descriptions of several land cover types, including urban, agricultural, and wetland, based on fieldwork and personal experiences. The analyst is looking for specific training sites representative examples of well-known land cover types within the remotely sensed data. For these training locations, multivariate statistical parameters are produced. Every pixel inside and outside the training locations is assessed and categorized according to its chance of belonging to that group. The creation of the Land use map has been in severe need of supervised categorization. The selected training courses included full user-visual interpretation assistance. Training sites are the regions that an analyst chooses within a picture to

represent the relevant land cover classes. For each training site, close to 30 example plots from the same land use land cover categories have been gathered and then combined into a single class. The study used the Maximum Likelihood Classification (MLC) approach. For this, a collection of model parameter values that maximizes the likelihood functions is chosen by the likelihood itself. Recoding was done to enhance the categorization results. The maps of LULC have been used to derive the urban area. Predicting the growth pattern's direction is possible by overlaying every extracted urban region. For detecting LULC change, many supervised classification techniques are employed.

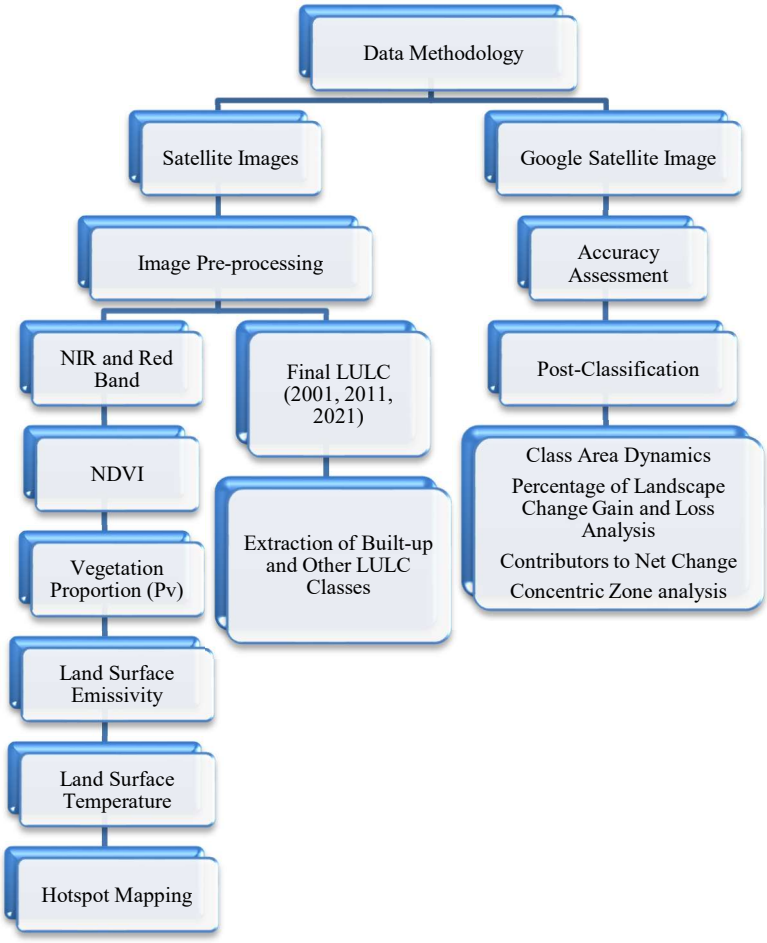

The CA-Markov model is a module that combines cellular automata (CA) with Markov Chain analysis for multi-criteria evaluation. It uses a CA function to project a future land-use map and applies Markov chain analysis with a contiguity kernel to estimate the projected land-use change. Specifically, the focus is on the transition area matrix. This module's knowledge and correctness will be evaluated and put on display. Considering both remote sensing and GIS data can be successfully integrated, this model may be a reliable method for both the spatial and temporal dynamic modeling of LULC and its quantity estimation. The definition of initial circumstances, parameterization of the Markov-CA model, analysis of transition probabilities, and development of neighborhood rules using transition potential maps are frequently done using biophysical and socioeconomic data.

Local rules defined by the CA spatial filter or transition potential maps control the spatial dynamics in the CA-Markov model. The Markov Chain, which is based on transition probabilities, controls the temporal dynamics between the land use/cover categories.

This spatial statistical model used to describe the dynamics of land use change and future forecast of land use is the Markov chain model. The foundation of this model's theory is the flow of data from Markov stochastic process systems in predicting status conversion. For each land-cover class, this model offers a series of conditional probability pictures. It is often employed in forecasting geographical characteristics that do not experience after-effect events, and it has developed into a crucial forecasting technique in geographic study. This model uses a Markov chain to anticipate changes in the future by taking into account different land-cover classes using satellite data and analyzing future simulations across two time periods (2001–2011 and 2011–2021) in IDRISI Selva.

Markov chains can be written as follows [Fan et al., 2008]:

$$P\left(x_t = \frac{j}{x_0} = I_0, X_1 = i_1, \ldots, X_{t-1} = i_{t-1}\right) = P\left(x_t = J / X_{t-1} = i_{t-1}\right)$$

If the discrete value was a_1……. and appears in a Markov chain of random variations, then

$$P\left(x_n = a_{in} / x_{n-1} = a_{i_{n-1}} \ldots, X_1 = a_{i_{n-1}}\right) = P\left(x_n = a_{i_n} / X_{n-1} = a_{i_{n-1}}\right)$$

The change matrix in the meeting Markov chain is tested using the chi-square (X2-test), which is written as follows:

$$\sum_{i=1}^{r} \sum_{j=1}^{c} \frac{\left(Q_i j - E_{ij}\right)^2}{E_{ij}}$$

Where r refers to the no. if row and c refer to the no. of column ij=Cell its actual number (r-1) * (c-1) is the degrees of freedom, and Eij refers to the expected value in cell ij.

Data Processing:

Image Pre-Processing:

For this study, Landsat images from 2001 to 2021 at the interval of 10 years were collected from the United States Geological Survey (USGS) website for analyzing the spatial-temporal changes in LULC and governing urban area expansion in the research region. The geometric correctness of each scene was confirmed, and all data were projected based on WGS 84, 45 N. Surface reflectance data have undergone post-production processing that included atmospheric correction, geometric correction, and other changes and are now available for use (http://landsat.usgs.gov/CDR_LSR.php). The CA-Markov model is a computational framework that integrates cellular automata (CA) with Markov Chain analysis to evaluate multi-criteria. The system employs a cellular automaton (CA) function to forecast a forthcoming land-use map. It utilizes Markov chain analysis with a contiguity kernel to approximate the anticipated land-use transformation. More precisely, the emphasis is on the matrix of the transition area.

Landsat 5 (TM) and Landsat 8 (OLI/TIR) sensors are used to analyze this study's disparity in urbanization levels between peri-urban and urban regions. ArcGIS 10.7 and QGIS 3.18.1 were used to gather, pre-process, and analyze the images for the years 2001, 2011, and 2021 to prepare them for land use.

Using a high-resolution Ortho-rectified image, the images were geo-rectified. Thematic Mapper (TM) and thermal image analysis are used to analyze the remote sensing data after pre-processing. Multi-spectral indices such as the Normalised Difference Vegetation Index (NDVI), Modified Normalised Difference Water Index

(MNDWI), and Normalised Difference Built-up Index (NDBI) are derived from TM and OLI images. **Table 1** provides a comprehensive overview of the technical parameters for Landsat 5 TM, Landsat 7 ETM+, and Landsat 8 OLI/TIRS.

Band	Landsat 5/7		Landsat 8	
	Wavelength	Resolution	Wavelength	Resolution
Band 1	0.45-0.52 (Blue)	30 m	0.43-0.45	30 m
Band 2	0.52-0.60 (Green)	30 m	0.45-0.51 (blue)	30 m
Band 3	0.63-0.69 (Red)	30 m	0.53-0.59 (green)	30 m
Band 4	0.77-0.90 (NIR)	30 m	0.64-0.67 (red)	30 m
Band 5	1.55-1.75 (SWIR)	30 m	0.85-0.88 (NIR)	30 m
Band 6	10.40-12.50 (TIR)	120 m	1.57-1.65 (SWIR 1)	30 m
Band 7	2.09-2.35	30 m	2.11-2.29 (SWIR 2)	30 m
Band 8	0.52-0.90 (Panchromatic)	15 m	0.50-0.68 (Panchromatic)	15 m
Band 9	-	-	1.36-1.38 (Cirrus)	30 m
Band 10	-	-	10.60-11.19 (TIRS 1)	100 m
Band 11	-	-	11.50-12.51 (TIRS 2)	100 m

Synthesis of Spectral Indices:

In the last few decades, change detection has also been done based on remote sensing data, which is primarily used to evaluate environmental processes both worldwide and locally. Monitoring, categorizing, and assessing the region may all be done with the help of the Landsat satellite. Red, green, and blue (visible band), infer red, near infer red (NIR), middle infer red (MIR), short wave infrared (SWIR), panchromatic, and thermal bands are among the bands that make up Landsat. Landsat 8 has 11 bands, compared to Landsat 5's 6 bands. Only a few bands (GREEN, RED, NIR, SWIR, or MIR) are employed for the spectral analysis of NDVI, MNDWI, and NDBI.

The Normalised Difference Vegetation Index (NDVI):

This index was developed by Rouse et al. in 1973 and is used to quantify vegetation by using near-infrared and red bands.

To observe greenery, NDVI is primarily employed as a vegetation index. Healthy vegetation acts as an excellent electromagnetic spectrum absorber in the visual range. Healthy plants exhibit a high Near Infrared (NIR) reflectance between 0.7 and 1.3 µm. The two bands utilized to compute NDVI are NIR and Red. The vegetation index was calculated using the following method; Equation (a) is for Landsat 5 and Equation (b) is for Landsat

8.

(Band 4–Band 3)/ (Band 4+ Band 3) ……(a)

(Band 5 – Band 4)/ (Band 5+ Band 4) ……(b)

The value of the NDVI index value ranges from -1 to 1. As the NDVI value is near 1, plant density rises as well. According to Akbar et al. 2019 and Bhandari et al. 2012, the NDVI values between -1 and 0 represent water bodies, values between -0.1 and +0.1 represent barren/semi-barren land and sand, the values between 0.32 and 0.5 represent agriculture shrubs and grasslands, and for dense vegetation or tropical rainforest the NDVI ranges from 0.6 to 1

MNDWI, or Modified Normalised Difference Water Index:

An MNDWI was obtained using the middle infrared and green bands. According to Hanqiu Xu (2006), it is typically used to reduce noise from populated areas.

Modified Difference The water spread area is located using the Water Index. A red and green band was applied. Water bodies often reflect little light. Only the visible range of the electromagnetic spectrum is reflected by it. In comparison to the green (0.5-0.6 µm) and red (0.6-0.7 µm) spectra, the blue (0.4-0.5 µm) spectrum exhibits a higher level of light reflection in liquid water bodies. Clearwater is the most reflective in the blue region of the visible light spectrum. Visible spectrum reflectance is increased in turbid water. Beyond near-infrared (NIR), there is no reflection. Gao (1996) suggested using the NDWI to construct water-related land-use/land-cover characteristics. The quality of the index result produced by NDWI is lower. Neither NIR nor SWIR is reflected by clear water. The GREEN band and SWIR band were used in the modified index, which made it superior to the other indices available in terms of improving water bodies. (Mukherjee & Samuel 2016; Szabo et al. 2016; Hanqiu Xu 2006). Water bodies will result from positive MNDWI values (0 to 1), whereas negative values (-1 to 0) correspond to either of the two forms of land use. The MNDWI is shown below for Equations (c) and (d), respectively, for Landsat 5 and Landsat 8.

(Band 2 – Band 5)/ (Band 2 + Band 5) …… (c)

(Band 3 – Band 6)/ (Band 3 + Band 6) …… (d)

Normalized Difference Built-up Index (NDBI):

The Normalised Difference Built-up Index (NDBI), which was first developed by Zha et al. (2003), is utilized to precisely extract built-up land (Dhar et al. 2019; Rasul et al. 2018; Xiong et al. 2012; Xu 2008; Zhou et al. 2014). The index ranges from -1 to +1, In the Near Infrared (NIR) and SWIR1 bands of the Landsat TM / OLI sensor data, built-up land exhibits a considerable increase in their reflection. For the examination of developed land, there are several indices. Modified Difference For the extraction of built-up regions Built- up Index (NDBI) is mostly used. Buildings and barren ground reflect more SWIR than NIR light. On the infrared spectrum, the water body doesn't reflect anything. NIR reflection is greater than SWIR reflection in the case of the greenie surface. With just a greater positive value signifying built-up and undeveloped land, the built-up index is a binary picture that automatically maps the built-up area.

(Band 5 – Band 4)/ (Band 5 + Band 4) …… (e)

(Band 6 – Band 5)/ (Band 6 + Band 5) …… (f)

For the data from Landsat 5 and 8, equations (e) and (f) are utilized to derive the built-up index. The range of the NDBI values is from -1 to +1. A value close to +1 indicates the high density of the build-up area, and a lesser number corresponds to aquatic bodies. The vegetation NDBI data have little importance.

Land Surface Temperature (LST) Derivation:

The LST derivation was conducted to determine if the LULC alterations had an impact on the thermal environment. The secondary information is required to prepare the LST. To guarantee the comparability of the approach, the Landsat imageries utilized for the LST derivation match the years in which LULC categorization was completed. Using QGIS and ERDAS imagining software, Adaptive filtering, fast Fourier transformation (FFT), and top atmospheric correction (TOA) are applied to the Landsat datasets to reduce noise. For LST, noise reduction is essential since it influences brightness temperature. Using an orthorectified high-resolution picture, multi-temporal Landsat Thematic Mapper (TM) and OLI/TIRS images were georeferenced. The RMS error for the picture is 0.26 and the thermal bands are resampled on 30m.

The temperature bands for conversion are provided in Equations (g) and (h) below.

$$L_\lambda = \frac{L_{max} - L_{min}}{QCAL_{max} - QCAL_{min}} * (QCAL - QCAL_{min}) + L_{min} \quad \text{(g)}$$

QCALMIN is the minimum quantized calibrated pixel value (corresponding to LMIN) in DN, which is 1 for LPGS products, 1 for NLAPS products processed after 4/4/2004, and 0 for NLAPS products processed before 4/5/2004. LMIN and LMAX are the spectral radiances scaled to QCALMIN and QCALMAX, respectively, in watts/(m^2*sr*µm) and watts/(m^2*sr*µm) respectively. The highest quantized calibrated pixel value (QCALMAX) in DN=255 is the same as LMAX.

$$T_k = \frac{K2}{\ln\left(\frac{K1}{L_\lambda} + 1\right)} - 273.15 \quad \text{(h}$$

Where, T_k is temperature represents a brightness temperature in Kelvin(k), Lλ-spectral radiance at the sensor's aperture unit of (W/m^2*sr*µm), K1: Calibration constant 1 in W/(m^2*sr*µm), K2: Calibration constant 2 in Kelvin (k). Table 2 shows the k–k-values of different sensors.

Thermal band calibration constant			
Sensors	Bands	W/(m²*sr*µm)	Kelvin
		K1	K2
TM	6	607.76	1260.56
ETM+	6	666.09	1282.71
TIRS	10	774.89	1321.08
TIRS	11	480.89	1201.14

Results and Discussion:

Urban development is currently one of the most crucial global challenges, of late, planners are interested in urban and environmental-related issues and paying more and more attention to understanding how urban structure is changing in the new era for sustainable development. The primary factors contributing to the escalating, uncontrolled expansion of cities are overpopulation, economic growth, and the integration of rural and urban areas. This phenomenon poses significant environmental and social risks, diminishing the quality of life in both urban and non-urban communities, and also leads to alterations in the spatial organization of cities.

The relentless process of urban expansion is inevitable. Still, it is crucial to foresee the future growth of cities to effectively plan and make policies that address the challenges arising from rapid urbanization. It is essential to comprehend and anticipate the alterations in land use and urban expansion to safeguard suburban areas, effectively manage environmental resources, and implement sustainable policies. Recognizing the possible effects on people and socioeconomic resources, as well as reducing the adverse impact on the environment, is part of this.

Extraction of LULC Classes and Maps:

For 2001, 2011, and 2021, images were collected and analyzed using the ARC GIS. For the extraction of LULC, supervised methods utilizing a maximum likelihood classifier algorithm were used. Anderson et al. (1976) proposed a system for categorizing land cover in remote sensing data, which involved modifying the existing approach. Urban (built-up), agricultural, vegetated, homestead, fallow, bare, water, and wetland areas were the eight classifications for LULC extraction (Table 1).

The study's primary objective was to map and analyze the progression of urban expansion and development. Given Jhapa's prominence in tea cultivation, it has been designated with a distinct land use classification. The TerrSet software's land change modeler (LCM) is utilized to analyze temporal changes and transitions in land use and land cover (LULC). After preparing the LULC map, a classification accuracy assessment is required.

Using a random sampling process, we evaluated the accuracy of LULC maps. On the other hand, the resolution of the satellite images severely reduced the accuracy. The researcher randomly chose seventy-four sample locations to assess the accuracy of the land-cover classifications for each of the seven classes. They settled on an accuracy assessment to measure total precision, user accuracy, and producer accuracy. Given the lack of current land-cover data, they supplemented it using field observations and Google Earth photos for

confirmation.

LULC Pattern 2001-2021:

The original plan was for the researcher to look at 2001 Landsat images to see how land usage changed that year. Numerous land use categories were established and used as examples for 2001. The ground truth verification validated the detected land use patterns. The reason is that preceding ground verification data is crucial for identifying the land use class pattern in supervised image classification. While classifying the picture, the researcher identified each pixel based on its color tone, texture, and ground truth information to verify each land use category. Figure 1 shows the eight categories that made up the land use pattern during the year. Following the supervised categorization, the estimated land area for this municipality was 1787.37 sq. km. According to the specified land use categories, vegetation occupied most of the study region (29%) followed by agricultural land (28%) and then built-up areas (17%) and homesteads (10%), as shown in Table 3.

Pattern of Land use and Land cover (sq.km)

LULC Classes	2001	Percentage	2011	Percentage	2021	Percentage
Agriculture	513.24	28.71	431.23	24.13	290.46	16.25
Bare Land	61.77	3.46	87.37	4.89	38.97	2.18
Builtup	319.51	17.88	411.35	23.01	543.91	30.43
Fallow Land	23.26	1.30	40.13	2.25	23.32	1.30
Homested	184.79	10.34	379.09	21.21	262.24	14.67
Vegetation	530.91	29.70	262.56	14.69	452.6	25.32
Waterbody	92.04	5.15	116.79	6.53	109.21	6.11
Wet Land	61.85	3.46	58.87	3.29	66.68	3.73

Table No. 3

Pinkish patches represent built-up regions, which were more noticeable in this municipal area as seen in Figure 1. Agricultural land was abundant during this historical period, as indicated by the golden color. Compared to neighboring places, the southern side has a higher proportion of agricultural land (Fig. 1). Due to the poor resolution of the picture, this period has a higher percentage of agricultural land than the previous periods.

Following the categorization of land uses in 2011, the land use pattern in 2011 (Fig. 1) was visually interpreted. In all, 8 different land use categories were found during the 2011 picture categorization process. According to 2011 image categorization findings, agricultural (431.23 sq km, or 24% sharing the total land area) came in first, followed by built-up areas (411.35 sq km, or 23% of the entire area), homestead land (379.09 sq km, or 21%), and vegetation sharing 262.56 sq km, or 14%, in that order (Table 3). The municipality's advantageous position, proximity to the nearby train station, a good market facility, both types of well-connected highways (metalled and arterial roads), and a solid infrastructure facility were the key drivers of the expansion of the built-up area.

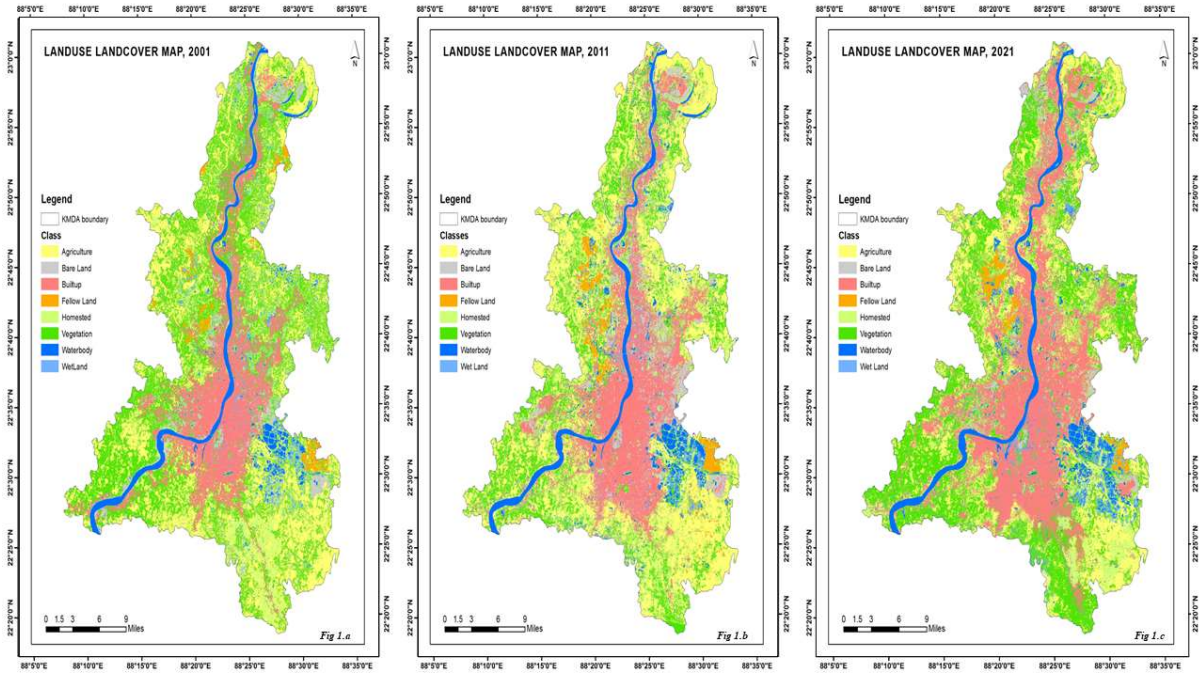

Buildings comprised 30% of the study area in 2021 (Fig. 1a-c), whereas vegetation, agricultural land, and homesites comprised 25%, 16%, and 14% of the area, respectively (Table 3). The southern part of this figure has a significant concentration of built-up area. Due to its proximity to the city center through the N.S.C. Bose Road, it is more expensive than other regions. In addition to these elements, metro rail is another reason for the region's extremely high population density. Following the year 2000, additional mouzas were added to this municipality's boundaries. It has been observed that the right side of the railway track is denser than the left side after the inclusion of those panchayats. because the railway track's left side is already very thick from previous years.

Land use cover Change detection:

The primary objectives of this research are to comprehend and measure the patterns of land use and land cover (LULC) and to forecast their impacts. Understanding the importance of land cover changes on a regional basis is crucial since it will make it easier to quantify changes over time and analyze them in terms of change rate. By observing and tracking a feature or phenomenon through time, change detection is the act of identifying changes in its state. In a setting where there is a risk of dynamic change, change detection in LULC might be performed annually. Analyzing the geographic scope of the shift in land cover classes allows one to gauge the magnitude of change. To track the severity of changes in the LULC pattern in the research region, three time-sequentially classed photos from 2001, 2011, and 2021 were utilized.

Examining the process of detecting changes in different land cover categories over time is a widely used approach for understanding the characteristics of the shift. These trajectories are characterized as patterns across time, which are in charge of altering the dynamics of earth resources in a certain region. These changes take place as a result of evolving local and regional conditions based on a variety of causes. A series of changes in land usage throughout a region can be used to identify the general pattern of change. In this work, land-cover change trajectories are produced, referring to consecutive land-cover types for a specific pixel across the observation period. A categorized map is generated as a result of post-classification change detection, which shows the sharing of land-cover classes for each pixel at two different periods. The "from" and "to" identifiers enable the establishment of a consistent path for land-cover transformation. Terrain The variations in the cover of a region are typically distinct, resulting in an intricate landscape with a diverse range of cover types (Clarke

et al., 1997).

Studying land-cover-changing processes is crucial since it provides a comprehensive understanding of the underlying factors behind these changes and enables predicting future outcomes. There are three distinct change trajectories: unmodified, stable, and unstable. The researcher generated Temporal change trajectories for each class to assess the region's evolving pattern of geographical distribution.

Magnitude of Landuse-Landcover Change (sq.km)			
LULC Classes	**2001-2011**	**2011-2021**	**2001-2021**
Agriculture	-82.01	-140.77	-222.78
Bare Land	25.6	-48.4	-22.8
Builtup	91.84	132.56	224.4
Fallow Land	16.87	-16.81	0.06
Homested	194.3	-116.85	77.45
Vegetation	-268.35	190.04	-78.31
Waterbody	24.75	-7.58	17.17
Wet Land	-2.98	7.81	4.83

Table 4

Based on the information in Table 4, the relative change in the municipality's land uses was evaluated. In this research region, the relative changes between 2001 and 2021 revealed some erratic patterns. Except for the built-up area, the land use change between 2001 and 2021 showed negative trends in most of the categories. Approximately 222.78 sq. km of agricultural land was lost between 2001 and 2021, whereas 78% of the natural vegetation was converted to built-up areas during this time. A total of 132.56 square kilometers of built-up area has been added between the years 2011 and 2021, while 116.85 square feet of homestead land have been turned into marshland or built-up area. In 2001, urban expansion resulted in a loss of 2.89 sq. km. of wetland. These are the effects of the area's rapid urbanization.

The urban area expanded by around 224.4 sq km between 2001 and 2021, whereas vegetation area declined by 78.31 sq km, water body increased by 17.17 sq km, and fallow land increased by 4.82 sq km. In comparison, between 2001 and 2011, urban and built areas grew from 91.84 square kilometers to 132.56 square kilometers, with the biggest growth being between 2001 and 2021. By contrast, vegetation, bare land, and agricultural land shrank. From 2001 to 2021, the most critical factor in the growth of cities, according to their results, was the transformation of farmland and desert into housing and other urban amenities.

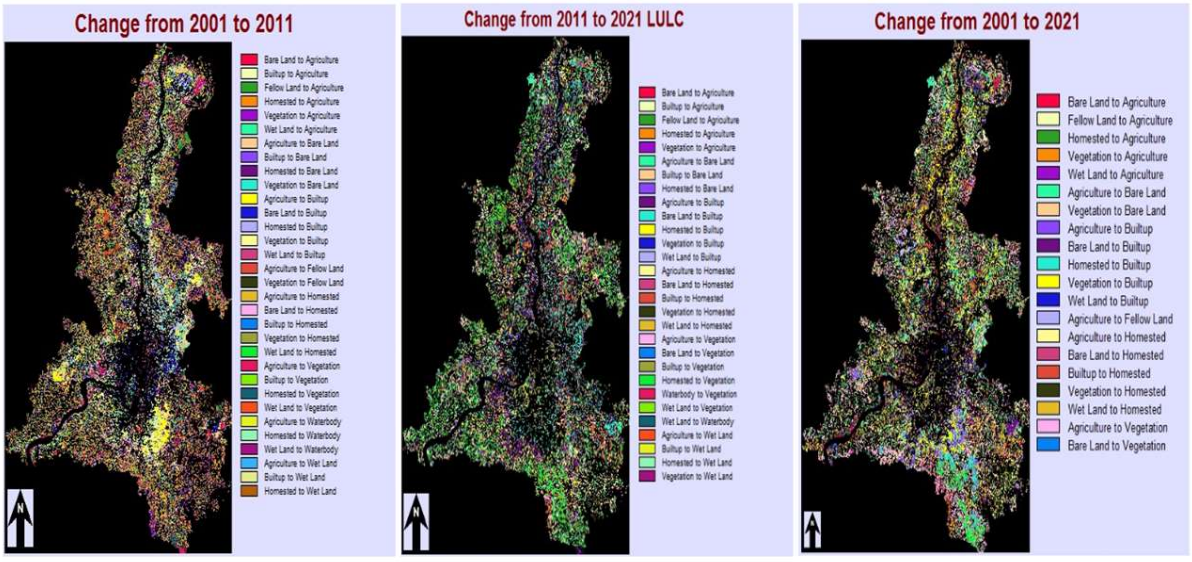

Fig 2.a Fig 2.b Fig 2.c

Accuracy Assessment of LULC Dynamics:

The secondary information that was utilized to create the LULC. To determine the final criteria for the various LULC classes, the ensemble of spectral indices is employed in the construction of LULC. This is done by applying the appropriate threshold values for each index. The Ground Control Points that were gathered as the study's core data were used to validate the LULC classification that had been completed. The confusion matrix was used to calculate the kappa coefficient (k) once the accuracy evaluation was completed. Additionally computed were the producer's accuracy (PA) and the user's accuracy (UA). Following is a presentation of the equations (i–k):

$$Producer Accuracy\ (PA) = \frac{Total no of correct pixels in a category}{Total no of pixels of that category derived\ from the reference data (row total)} \quad \text{(i)}$$

$$User Accuracy (UA) = \frac{Total no of correct pixels in a category}{Total no of pixels of that category derived\ from the reference data (column total)} \quad \text{(j)}$$

Any categorization project must include an accuracy assessment. It makes an accurate comparison between the categorized image and another data source. Only situations that may have been appropriately categorized by accident are controlled by Kappa.

row total row total maps have an overall classification accuracy of 94.6% for 2001, 94.6% for 2011, and 97.33% for 2021. According to the findings, categorized satellite images are suitable for accurate and efficient modeling of changes in land use and land cover. Additionally, between 2001 and 2011, producers had a perfect % accuracy rate of 100% when it came to categories including built-up areas, fallow land, homesteads, water bodies, and wetlands, according to a study that examined user and producer precision. In 2021, all categories

except agriculture and bare ground are projected to achieve the highest level of accuracy at 100%. The producer accuracy for bare land in 2001 was the lowest (84.62%). Agriculture (100 percent, 2001), bare lands (100 percent, 2011), and built-up regions (100 percent, 2011) had better user accuracy than water bodies and wetlands. The Homestead had the lowest user accuracy (60%, 2021) (Table 5).

Between 2001 and 2021, there were several notable changes in land use. Urban areas consistently increased, while arable land showed a gradual decline. The number of woods and bushes remained unchanged. Water bodies and wet regions exhibited non-linear increases. There was no general deterioration in the availability of permanent water resources, notwithstanding several periods in which the water bodies shrank. Instead, seasonal variations in rainfall dictated the amount of land that was covered by water.

Spatial Trend Analysis:

Spatial Transition of Landuse - Landcover

	LULC	Agriculture	Bare Land	Builtup	Fellow Land	Homested	Vegetation	Waterbody	Wet Land
2001-2011	Agriculture	269.144	23.3403	40.0176	15.3672	111.04	37.2571	6.04466	10.6071
	Bare Land	12.8272	20.5075	17.5654	0.0172445	6.54799	1.6405	1.50825	1.14654
	Builtup	10.5186	11.2311	235.673	0.0719524	19.3174	22.7379	3.56741	16.3903
	Fellow Land	6.63972	0.0011	0.581385	11.113	2.09368	0.78546	0.908981	1.12068
	Homested	35.6863	5.96338	35.6735	3.79285	45.2499	44.3462	5.33776	8.64626
	Vegetation	88.5213	23.9117	71.0955	8.18595	187.615	141.962	2.99043	6.33542
	Waterbody	1.72083	0.872853	1.7117	0.116433	1.16726	1.50415	81.5906	3.34118
	Wet Land	5.77479	1.51739	9.00229	1.4417	5.81632	12.1782	14.8236	11.2584
2011-2021	Agriculture	199.999	11.3473	64.6078	1.61847	71.9128	67.6057	4.44894	9.32777
	Bare Land	9.64923	13.1034	40.1447	0.269712	14.1739	7.84902	1.23525	0.918007
	Builtup	11.8871	5.60114	337.718	0.758807	24.0487	18.0355	3.32676	9.95249
	Fellow Land	10.2615	0.18784	2.11412	13.9166	4.5137	3.95885	1.72067	3.43892
	Homested	41.4275	5.54983	45.128	4.3704	100.159	175.572	1.58747	5.10626
	Vegetation	9.05414	1.9014	26.8585	1.17866	40.3987	166.126	2.28291	14.6268
	Waterbody	3.81268	0.74832	4.65835	0.471394	1.96138	5.92117	87.9116	11.2933
	Wet Land	4.13131	0.513895	22.6233	0.727774	4.95048	7.21434	6.68924	11.9991
2001-2021	Agriculture	192.775	12.4531	69.611	5.9193	77.0145	132.362	7.62339	15.0205
	Bare Land	5.46859	10.4185	27.6862	0.315639	7.72003	6.8604	2.22154	1.06678
	Builtup	4.39761	2.31005	259.585	0.0147966	18.7573	20.1693	3.39954	10.8729
	Fellow Land	6.66887	0.0941859	1.32646	8.13877	2.23563	1.8692	0.948198	1.95402
	Homested	21.322	3.82844	52.2849	2.12151	31.2009	59.498	4.58605	9.84993
	Vegetation	51.6021	8.28329	117.902	4.82408	118.705	216.619	3.04834	9.63933
	Waterbody	3.03086	0.50944	2.76705	0.111859	1.06653	2.91143	78.1444	3.48534
	Wet Land	4.90317	1.05318	12.6801	1.86304	5.38916	11.9338	9.22355	14.7659

Table 6

Due to many work possibilities in construction companies engaging locals as unskilled laborers and encouraging them to give up farming practices, agricultural area decreased throughout the evaluation period from 2001 to 2021 from 28.71% of the total area to 16.25% (Table 2). Due to the state government's strict measures for regenerating the badly degraded river floodplain, the built-up area did not change during that time. The net change and contribution of various land use types from 2001 to 2021 are shown in Fig. 3(a). Between 2001 and 2011, there was a greatest rise in housing stock and a maximum loss of vegetation. The transition of land use classes into settlement is shown in Fig. 3(c) from 2001 to 2021, which also shows the concentration of human activity in the flood plain of the Hooghly River.

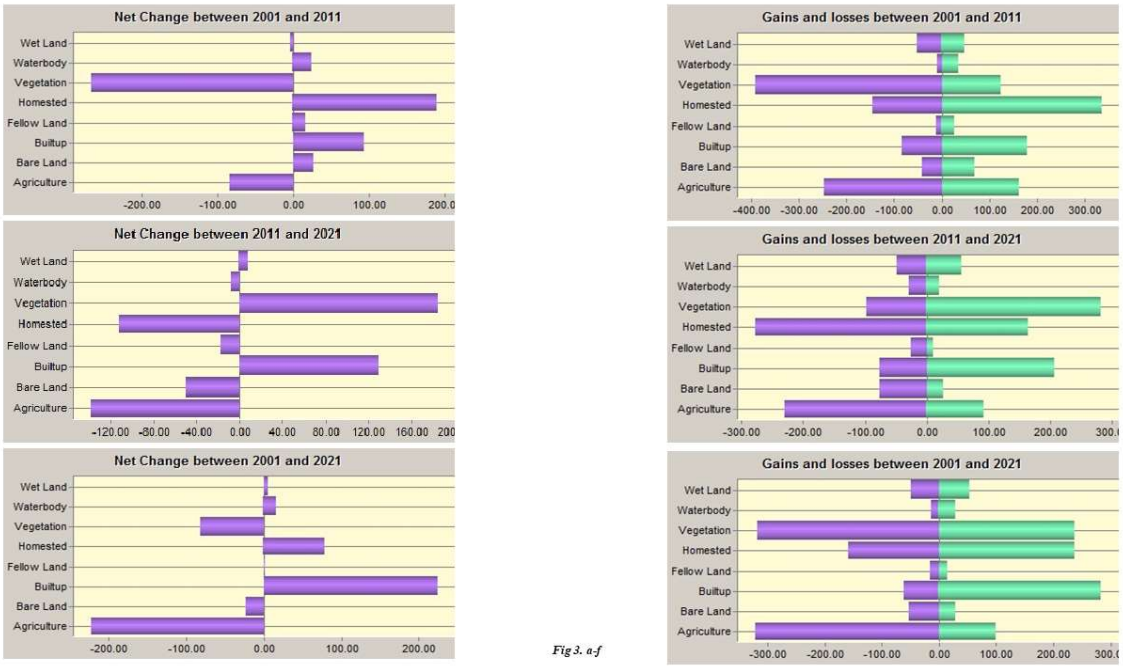

Fig 3. a-f

LULC has changed due to human activities and natural processes, with the specific ratios of transition varying across different historical periods. Figure 3a-f shows the changes in LULC (land use and land cover), including positive and negative effects, during the research project. There are three distinct phases to the LULC transition in the area.

In first stage covers the years 2001 to 2011, and during that time, there was a decrease in the amount of land that was farmed, from 513.24 km2 to 431.23 km2, mostly due to the conversion of 111.04 km2 to homesites, 40.02 km2 to buildings, 37.25 km2 to vegetation, 23.34 km2 to bare ground, and 10.61 km2 to the wetland area. A substantial decrease in vegetation from 530.91 to 262.56 km2 and an increase in the area of the homestead from 184.79 to 379.09 km2 were two additional significant changes (Figure 3a-b). This fall in vegetation was mostly caused by the conversion of 187.615 km2 of vegetation to homestead. A further four significant changes included a rise in the amount of bare land from 61.77 to 87.37 km2, which was primarily caused by the conversion of 23.9117 km2 of vegetation and 23.3403 km2 of cultivated land. From 23.26 to 40.13 km^2 of fallow land increased over this period, mostly due to the conversion of 15.37 km^2 of agricultural land, 8.18 km^2 of vegetation, and 3.79 km^2 of homestead land.

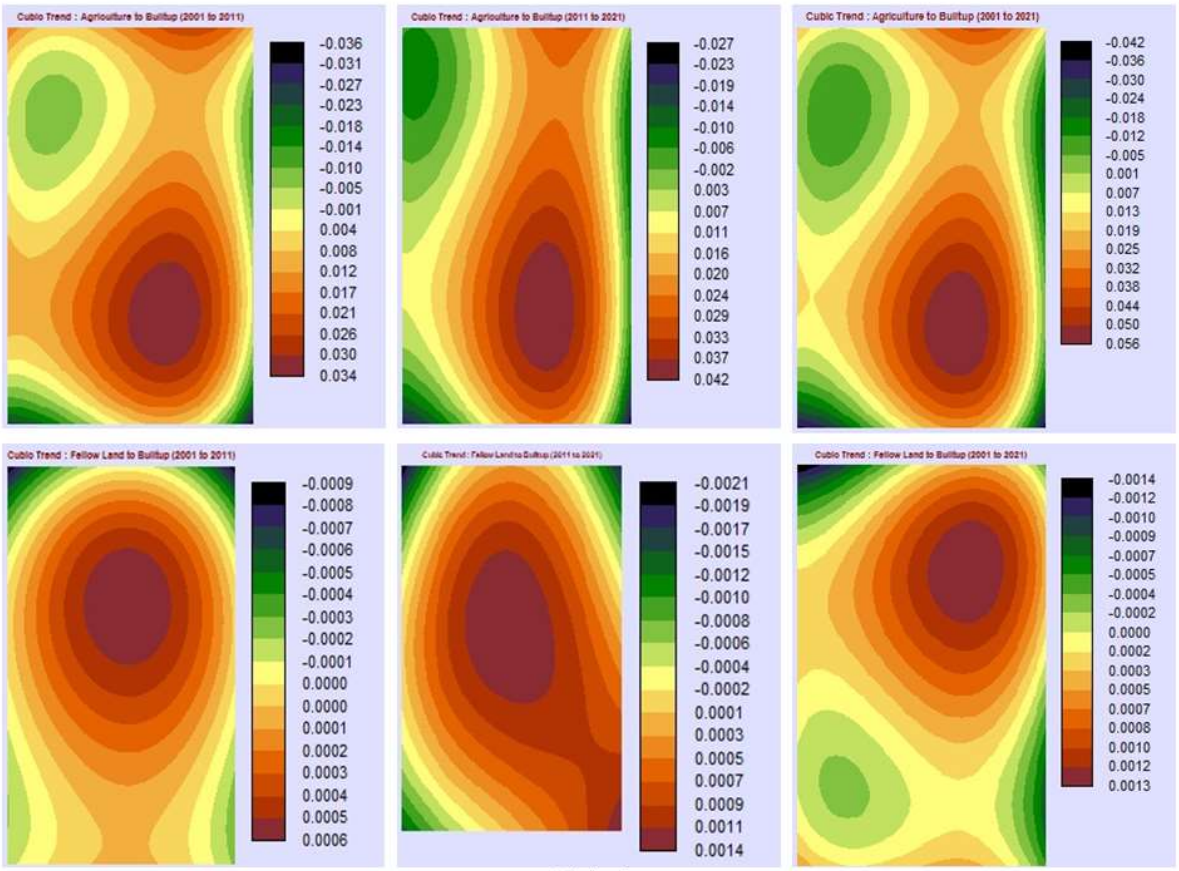

Fig 4. a-f

The urban area exploded between 2011 and 2021, rising from 411.35 km2 to 543.91 km2, at the expense of 64.6078 km2 of arable land. The loss of woodland (67.6057 km2), homesites (71.9128 km2), bare land (11.3473 km2), water (4.448 km2), and west land (9.33 km2) contributed to further reductions in cultivated land to 290.46 km2. Of this, 26.86 km2 of built-up land and 40.3987 km^2 of forest were converted (Figures 3c-d). The conversion of 14.63 km2 of vegetation and 11.93 km2 of waterbody to wetland contributed significantly to the growth in the wetland area from 58.87 to 66.68 km2 in the second stage. At the expense of 175.57 km^2 of homestead and 67.6057 km^2 of cultivated land, the vegetation area increased from 262.56 km^2 in 2011 to 452.6 km^2 in 2021.

From 2001 to 2021, the study's end period, urban areas increased from 319.51 to 543.91 km2, replacing vegetated land by 117.902 km2, agricultural land by 69.611 km2, bare land by 27.69 km2, and homestead land by 52.28 km2. The change from cultivated farms to vegetative land of 132.362 km2 revealed a sharp reduction in agricultural area from 513.24 to 290.46 km2. The conversion of 9.223 km2 of wetlands to water body delineated a rise in waterbody area from 92.04 to 109.21 km2, and the area of 118.705 km2 of vegetation to homestead land exhibited a strong growth in homestead area from 184.79 to 262.24 km2. (Figure 3e-f).

The generalized pattern of development between 2001 and 2021 is seen in Figures 4(a-f) and 5(a-c), with urbanization spreading out from the center. The more heavily altered sections, which are shown by the deeper red patches, gradually lessen as they approach the city's periphery. To show this cubic analysis, the LULC maps between 2001 and 2021 were used. The more heavily altered sections, which are shown by the deeper red patches, gradually lessen as they approach the city's periphery. Due to the conversion of agricultural land, the southeast has more urban areas.

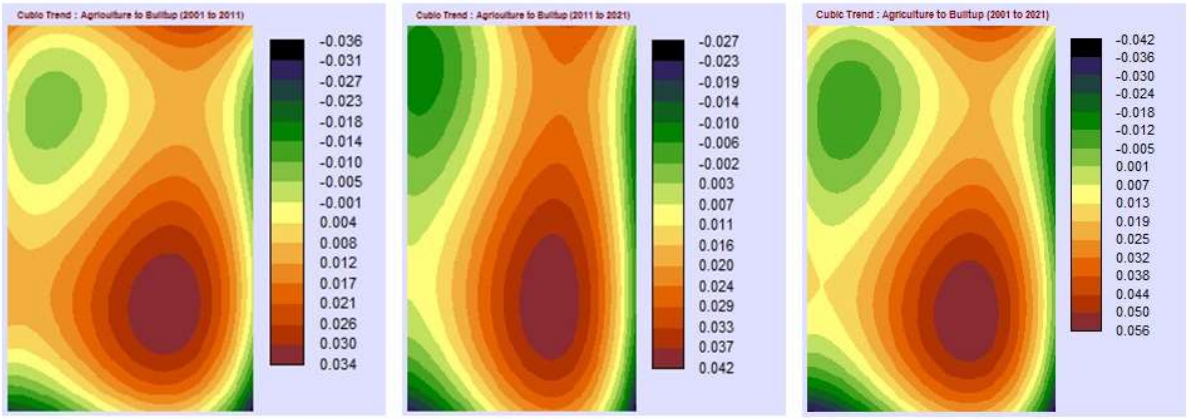

Fig 5. a-c

On the other hand, the overall pattern of change between 2001 and 2011 shows urbanization as a result of the conversion of fallow land moving towards the center, the darker red area concentrated towards the western part in the second period (2011–2021), and the urbanization moving towards the northern-eastern part in the final stage.

The overall pattern of development between 2001 and 2021 is seen in Figure 5(a-c), with urbanization spreading outward from the central area. The more heavily altered sections, which are shown by the deeper red patches, gradually lessen as they approach the city's periphery. Urban areas are more prevalent in the eastern, middle, and southern regions than in the western and northern ones.

Urban Expansion:

According to Hauser (1966), the process of urbanization can be clearly distinguished as a change in people's occupation from agricultural to non-agricultural (Singha, 1990) and it also brought about the concentration of population in a small area, implying high densities.

Burgess (1925) used a pattern of concentric circles to depict the process of urban growth in its optimum state. This circle is prone to expanding outside due to the encroachment of new outside (rural or fringe) land uses. This feature is referred to as succession in ecology. Thus, the opposing and complementary processes of concentration and decentralization serve to control the process of expansion. The city naturally gravitates toward the Central Business District or city center as a result of the close interplay between these two factors (Burgess, 1996). This area eventually becomes the center of political, cultural, and economic activity and might be considered the urban core. The most significant area of an urban region is its core, which is characterized by its central location despite its limited size. In addition to contributing to the city's physical growth, urban expansion possesses a significant impact on how society is organized (Burgess, 1996).

The process of urban expansion is driven by the relationship between the agricultural surplus and the growth of the manufacturing sector (Palen, 1992). Because the introduction of the urbanization process creates more and better employment opportunities with higher wages in the urban sector (Lewis, 1954; Fei and Ranis 1961; Todaro, 1976; Giri, 1998), the World Bank report (1982) demonstrates a closer relationship between the process of urbanization and shifting of the labor force. According to this theory (Mills et al. 1986; Giri, 1998), the process of urbanization results in a shift in job prospects from the mostly rural primary sector to the primarily urban tertiary sectors. People are drawn away from rural areas in emerging nations by factors including better work opportunities (Giri, 1998). The city region expands and spreads continuously as a result of the agglomeration of urban centers (TCPO, 2001). Peripheral zones have altered more quickly than other zones in metropolitan areas with quicker growth rates (Katz et al. 1994).

The largest cities in the world have been actively absorbing their outskirts since the turn of the 20th century and rapidly filling up with urban mass (Hoyt, 1966). Population growth, urbanization, and industrialization—three key elements of urban dynamics—have overlapping peaks that together produce the process of neo-urbanization (Guohua et al. 2007). Neo-urbanization is characterized by its unchecked diversity and complexity. According to Fagan et al. (2001), urban expansion is a process of ecological colonization in which individual colonists (houses) seize the open space at the boundaries of the urban fringes and foster the ensuing growth gradually.

Several authors have drawn parallels between sprawl and the natural expansion of metropolitan regions in response to population growth, including Sinclair (1967), Brueckner and Fansler (1983), and Lowry (1988) (Marzluff et al., 1994; Ewing, 2008). Its spatial dimension undergoes arbitrary alterations (Peiser, 1984; Koening, 1989). Urban sprawl has been a problem in many cities in developing nations (Bhatta et al. 2010). It has standards that are distinct from those of the urban growth process, which may, in some situations, be planned. Urban sprawl may be distinguished from other types of spread based on examining its effects. urban development methods that are linked.

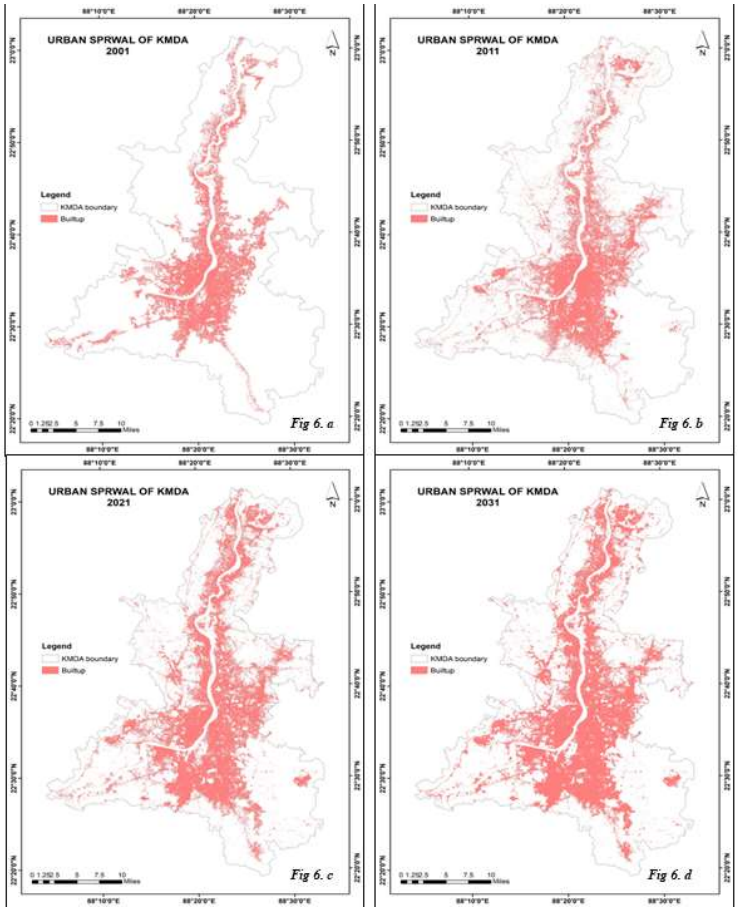

Urban sprawl, in the words of Marathe (2001), is a process "that has spiraled out of control." Unbalanced or unplanned haphazard expansion without any planning leads to urban sprawl. It has three dimensions, namely the dimensions of density, land use, and time. The unfavorable patterns of land use that characterize sprawl include continuous low-density development, leapfrog development, strip/ribbon development, and dispersed development.

As shown in Table 7, the region's urban area had a total size of 319.51 km2 in 2001 and had grown an average of 2.87% per year over the subsequent 10 years. Urban coverage was 411.35 km^2 in 2011; however, by 2021, it

had drastically expanded to 543.91 km^2, with approx annual urban growth rate of 3.22%. from 2001 to 2011, it grew dramatically, reaching 91.84 km^2. With an average yearly growth rate of 3.5%, the district's size increased significantly, growing by 224.4 km^2. This urban expansion lasted from 2001 to 2021. In the future, from 2021 to 2031, the urban area will reach nearly 607.77 sq. km area with 1.17% growth rate per year.

Years	Area	% of Area	Growth Rate
2001	319.51	17.88	
2011	411.35	23.01	28.744
2021	543.91	30.43	32.226
2031	607.77	34.00	11.741

Table 7

Driving forces, also known as the underlying elements (Rahaman, M.T. 2016) that initiate urban development, are in charge of the urban growth that takes place at certain temporal and spatial scales. For a better understanding of the elements that promote urbanization, context is necessary because they each play a varied function in a given time and place. Beijing's urbanization was primarily influenced by physical, socioeconomic, and neighborhood variables, with socioeconomic factors having the most influence overall, except for the first 12 years of the research period (1972 to 2010). Additionally, when the socioeconomic variables grew, the importance of physical and neighborhood characteristics decreased (Li, X.; Zhou, W.; Ouyang, Z. 2013). Greater Dhaka's urbanization was affected by several factors, including its physical environment, population expansion, and economic development (Dewan, A.M.; Yamaguchi, Y, 2009).

In Nepal, several factors, such as public service availability, economic prospects, population expansion, globalization, political circumstances, government strategies, social and cultural connections, and rural-urban connections, have notably impacted population movement [Rimal, B.; Baral, H.; Stork, N.E.; Paudyal, K.; Rijal, S. 2015]. In rural areas, 21% of migrants migrated for agricultural purposes, while 17% migrated for service-oriented purposes in urban areas, according to a 2014 CBS report [Rimal et al., 2017].

Factors such as population growth, geographical considerations, government policies and programs, the impact of globalization, and easier access to public services all contribute to the rapid urbanization of the Jhapa area. Opportunity, political atmosphere, and development programs in particular epochs bolster these factors even further. Other Nepalese cities also experience the same situations. Greater economic possibilities, accessibility to public services, and globalization are the primary factors influencing Pokhara's urbanization trend [Rimal, B. 2012]. The Kathmandu Valley's urbanization process was greatly influenced by economic possibilities in the center, population increase in the periphery, and political conditions in rural regions [Thapa, R.B.; Murayama, Y. 2010]. Similar to how physical circumstances, accessibility to public services, globalization, and plans and regulations all play a role in urban sprawl [Rimal, B.; Zhang, L. 2017].

Transition Probability Matrix& Predicted LULC:

The researchers created the transition potential matrix to predict the future changes in each type of land based on the LULC conditions over 2001-2011, 2011-2021, and 2001-2021. Off-diagonal data suggests the convergence of distinct occurrences, while data points on the matrix's diagonal indicate the persistence of a phenomenon throughout time. For instance, the transition probability matrix reveals that from 2021 to 2031, there was a 4.73% chance of losing cultivated land to a built-up area and a 23.64 percent chance of losing it to a vegetation area.

Probability of Changing in 2031								
LULC	Agriculture	Bareland	Builtup	Fallow Land	Homestead	Vegetation	Waterbody	Wetland
Agriculture:	0.5097	0.0254	0.0473	0.0094	0.1434	0.2364	0.0063	0.0221
Bare Land:	0.0917	0.2776	0.3879	0.0037	0.1412	0.0692	0.0266	0.0021
Builtup:	0.0021	0.0051	0.8776	0	0.0473	0.0344	0.0025	0.0309
Fallow Land:	0.2999	0	0	0.5089	0.0763	0.0004	0.0216	0.0929
Homested:	0.1148	0.0213	0.212	0.0104	0.1847	0.3772	0.0134	0.0662
Vegetation:	0.0844	0.0138	0.1282	0.0071	0.2798	0.484	0	0.0028
Waterbody:	0.0226	0.0041	0.0077	0	0.0012	0.0126	0.9208	0.0311
Wetland:	0.0629	0.017	0.1389	0.0328	0.0597	0.1744	0.1256	0.3887

Table 8

Table 8 indicates that unoccupied land has the most significant capacity to transform into developed regions over the projected timeframe. Furthermore, although other phenomena exhibited a greater probability of changing, metropolitan areas, fallow land, woods, and water bodies were more prone to staying consistent. Wetlands saw the highest drop throughout this period, whereas homesites saw the greatest rise.

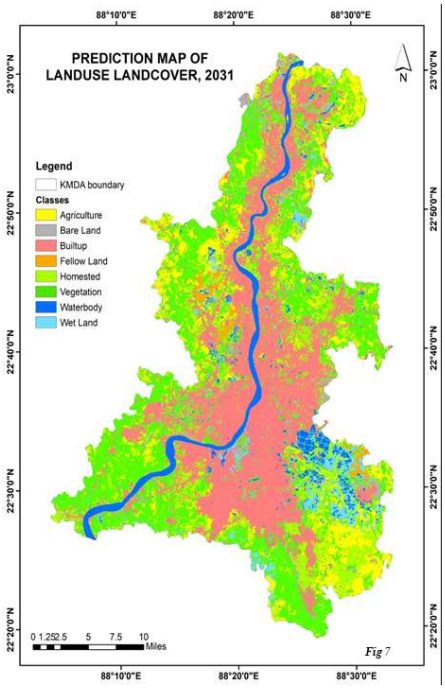

The predicted land usage for 2031 is shown in Figure 7 and Table 9 using the CA-Markov chain analysis. This map suggests that expanding built-up areas should be a problem for spreading development due to sustainable urban growth. To limit spreading growth, this forecasted map will help with developing future planning for built-up development.

LULC Classes	2031	Percentage
Agriculture	216.69	12.12
Bare Land	30.05	1.68
Builtup	607.77	34.00
Fallow Land	16.42	0.92
Homested	240.20	13.44
Vegetation	495.46	27.72
Waterbody	102.84	5.75
Wet Land	78.01	4.36

Table 9

Figure 7 illustrates the expected land use and land cover for 2031, with an estimated built-up land area of 607.77 sq. km. In the Kolkata Municipal Development Area, there are 216.69 sq km of agriculture, 495.46 sq km of vegetation, 102.84 sq km of water bodies, and 30.05 sq km of undeveloped land, respectively. The forecast has an error rate of 0.17%, making it reliable for providing accurate information on land use and cover.

Urban Heat Island:

Spatio-Temporal Analysis of NDVI:

NDVI Profile (2001-2021) Sq.km			
Zones	2001	2011	2021
Low	56.63	66.72	58.42
Moderately Low	199.19	442.10	60.59
Moderate	1026.07	1003.43	693.47
Moderately High	498.58	258.97	904.92
High	7.79	9.61	70.91

Table 10

All three images were density sliced into five classes as shown in Table 8 above for the determination of the temporal fluctuations of NDVI with time. The density sliced pictures for the years 2001, 2011, and 2021 are displayed in Figure 6(a-c). As can be observed, compared to 2001, the non-vegetated area has significantly risen in the 2011 photograph. The built-up region increasingly extends beyond the city's boundaries, particularly on the eastern and southern sides. Figure 8(a-c) depicts the city core (Kolkata and the surrounding regions) in 2001 with moderately low to moderate vegetation. By 2011, however, this vegetation had shifted to moderately low levels, and by 2021, most of it had become a moderately highly vegetated area.

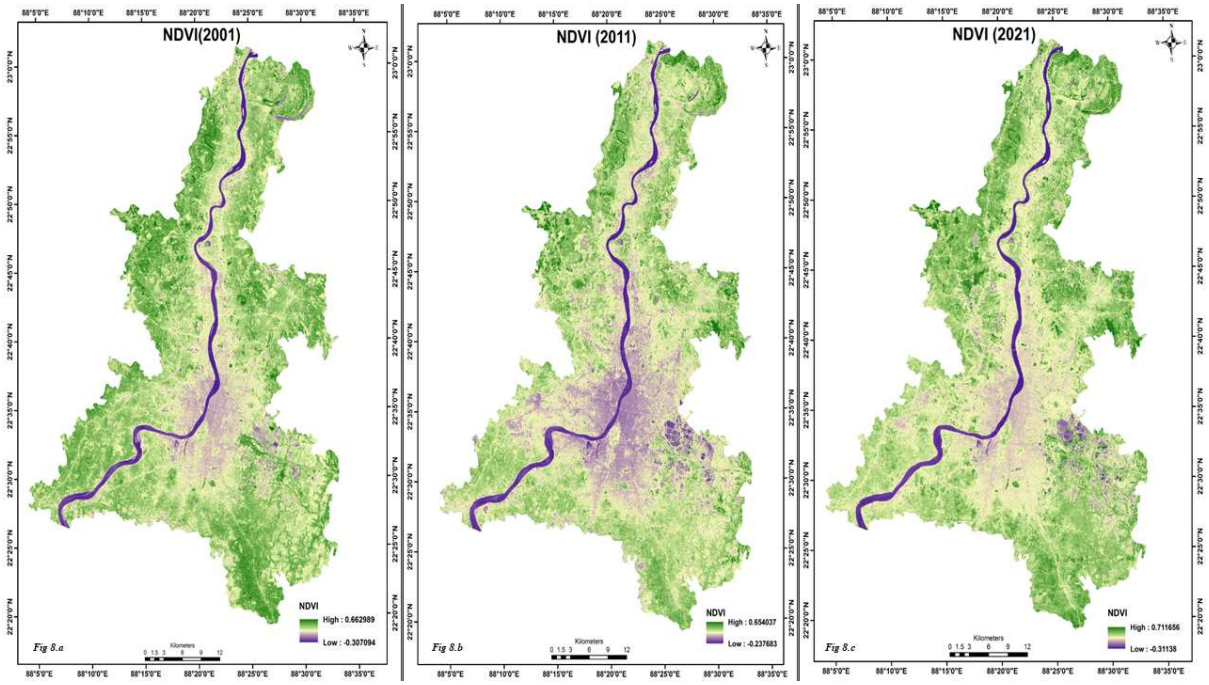

This is because formerly this area was covered with sparse vegetation and natural bushes, but with an increase in population, new residential complexes have been built here. Furthermore, because the city is a metropolis and urbanization is growing quickly, the vegetation cover was relatively low in 2011 but this vegetation cover rose as a result of a lockdown scenario in 2021.

Similar to the Madhyamgram-Barasat region in Figure 6(a-c), which is located in the eastern portion of the city, this area was formerly an agricultural one, but due to the city's growing population, practically the whole territory has been turned into a built-up area. The Sankrail region appears to be following a pattern in which the amount of moderate to thick vegetation has reduced between 2001 and 2011 (Figure 6b) and has also grown between 2011 and 2021 (Figure 6c).

Vegetation Content Ratio (P_V):

Using the NDVI results, calculate the proportional vegetation (Pv). The area estimated to be covered by each form of land cover is provided by this proportionate vegetation. Pure pixels are used to record the NDVI's vegetation and bare soil proportions. A range of NDVI from 0.5 to 0.2 has been proposed for situations on a global scale. In the case of higher-resolution Rsnge of NDVI in agricultural settings can approach 0.8 or 0.9, however, the value for vegetated regions (NDVI = 0.5) is considered low in some circumstances (Wang et al. 2015). Equation (L) may be used to determine Pv.

$$p_v = \left(\frac{NDVI - NDVI_{min}}{NDVI_{max} - NDVI_{min}}\right)^2 \qquad \text{(L)}$$

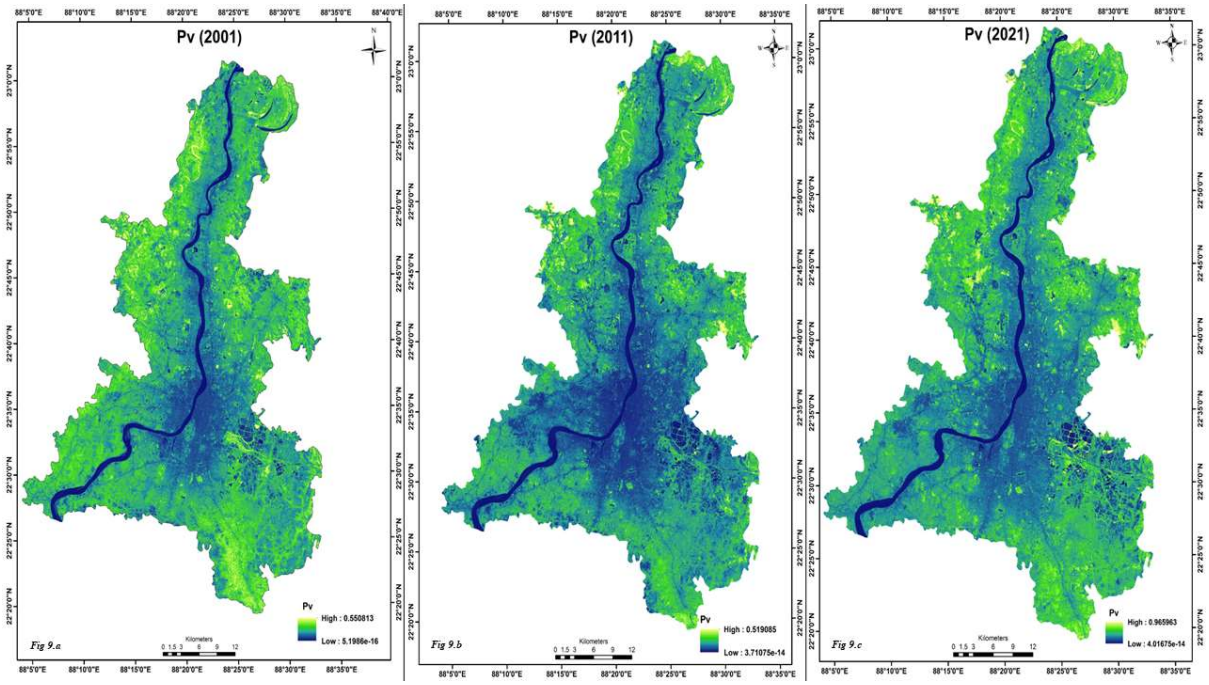

Image histogram statistics (max and min values) were utilized to estimate the percentage of plant cover from Equations (L). Using statistics, it was calculated that the NDVI values for vegetated and non-vegetated regions were 0.93 and 0.00, respectively.

Figure 9(a-c) demarcated the proportion of vegetation in the study area, where blue patches are represented as low Pv and light green to yellow patches represent high Pv. In the year 2001, light green to yellow shades of patches were found in the fringe area whereas in 2011 the city centre and surrounding town areas were concentrated in the blue patch due to covid lockdown in 2021 some parts of the western side had high Pvis found.

LST & LSE:

An emissivity-based NDVI has been calculated through three distinct scenarios (<0.2, 0.2-0.5, and >0.5) (Sobrino et al., 2004). The reflectivity values in the red zone are utilized to compute the emissivity values in the initial situation, which is conceptualized as an uninhabited landscape. Locations that usually have NDVI values exceeding 0.5 are associated with an emissivity rating of 0.99. Soil and vegetation are represented by NDVI values between 0.2 and 0.5. Therefore, Equation (m) was used to determine the surface emissivity:

$$\mathcal{E}=\mathcal{E}_{v}P_{v}+\mathcal{E}_{x}(1-P_{v})+d\mathcal{E} \qquad \text{(m)}$$

The vegetation proportion obtained is determined by the vegetation canopy emissivity (εv) and the bare soil emissivity (εs). dε is the internal reflection emissivity due to cavity effect dε=(1−εs) (1−Pv) Fεv.

To compute the LST from Landsat photos, an emissivity adjustment is more crucial (Srivastava et al. 2009). It was initially described by Gillespie (1985), and Li et al. (1999) recommended using it to quantify emissivity. Both Zhang et al. (2008) and Li et al. (2013) state that the method predicts the maximum temperature emissivity for each pixel. The surface emissivity is adjusted using Equation (n) (Zhang et al. 2013). This technique was used to calculate the emissivity values in areas where the NDVI is less than 0.4.

$$\varepsilon=0.004*p_{v}+0.986 \qquad \text{(n)}$$

Surface radiation detected by satellite sensors may be utilized to calculate Land Surface Temperature (LST) and emissivity across extensive areas. Since these measurements account for the entire surface, they are superior to point measurements taken from the ground in many contexts, such as those involving the Earth's radiation budget and climate change detection. Many people are interested in calculating LST and emissivity using data from passive sensors.

To measure how much heat radiation reaches the Earth's surface relative to how much heat radiation a black object emits at a given temperature, scientists measure land surface emissivity (LSE). The land surface characteristics are the primary determinants of LSE. LSE is a fundamental component of land surface temperature retrieval, and the quality of this component directly influences the algorithm's precision. To quantify land surface emissivity at the moment, visible light and near-infrared spectral data are mostly used.

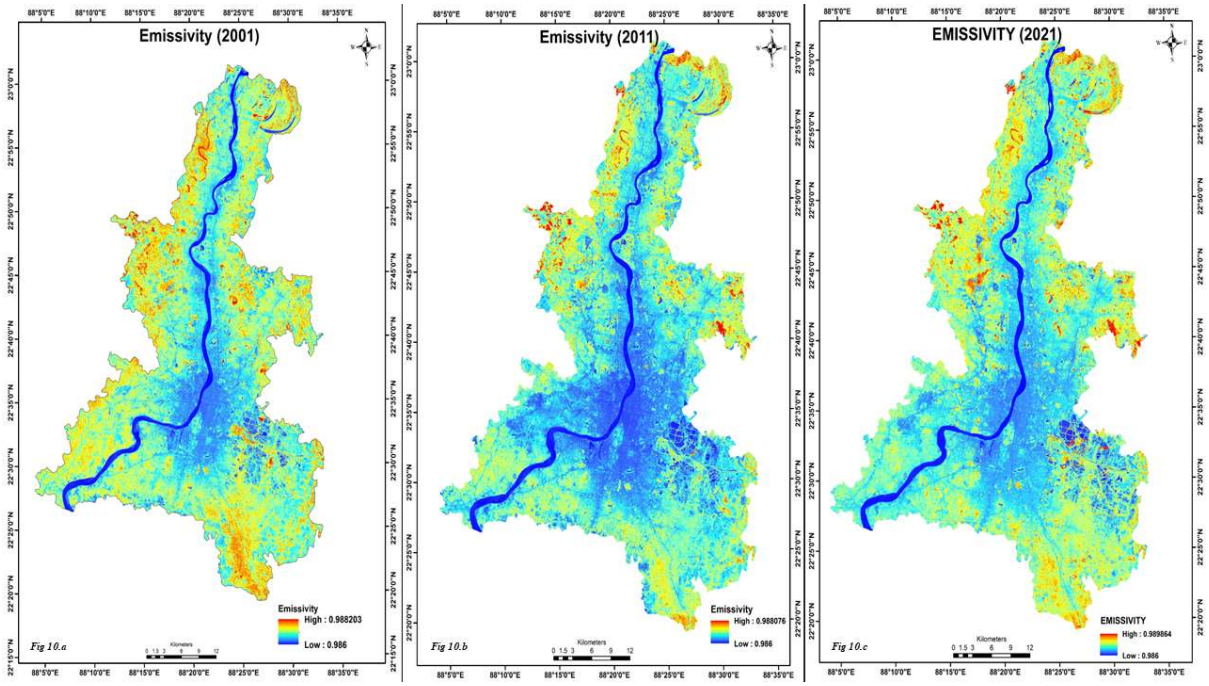

The lowest minimum value for Figure 10a for the year 2001 was 0.986, while the highest emissivity values were 0.988. This proved that a vegetated canopy may block short-wave solar radiation from entering the atmosphere. Because land absorbs heat more quickly than water, solar heating of the earth's surface is uneven, with air warming, expanding, and rising over land while cooling and sinking over colder water surfaces. High heat waves are also emitted by surfaces that are parallel to the sun's ray path and are unobstructed by structures or canopy cover (National Oceanic and Atmospheric, 2017).

The mean emissivity of the vegetated area was 0.9878 in 2011, which was the lowest value. In 2011, the mean emissivity values for water and open space were 0.9860 and 0.9867, respectively, while 0.9861 was the value for the built-up area.

The vegetated area's highest and minimum emissivity values in 2021 were 0.98881 and 0.9888, respectively. In the year 2021, the mean emissivity values for water and open space were 0.9860 and 0.9862, respectively. In the year 2021, the built-up area's mean emissivity rating was 0.9866. This was greater than the values for other forms of land use for the year 2021 but somewhat lower than the values for the years 2001 and 2011, as shown in Figure 10(a-c).

LST:

A growing percentage of the global population currently resides in urban areas, swiftly transforming the Earth's surface into urbanized zones. According to predictions by Pacione (2003), the worldwide urban population is expected to increase from the current pace of over 50% (about 3.5 billion people) to two-thirds of the estimated global population, which is 6.2 billion people, by 2050. By 2050, there will be 9.8 billion people on the planet, 6.2 billion of whom will live in cities. African and Asian populations are predicted to make up the majority of the world's 2.3 billion inhabitants by 2050 due to their rapid average yearly growth. Furthermore, 16 of the 29 greatest megacities in the world are expected to be in Asia by 2025. Asia's population growth rate would be substantially larger than that of any other area of the world and historically unmatched. Such massive changes to the earth's surface directly affect the environment, which is affected in different ways and to varying degrees. Urbanization modifies the biophysical characteristics of cities at the microscale by modifying the local climate. Cities' local climate is interconnected with the regional and global environment through the intricate chemistry of air processes affecting radiation balance and greenhouse gas emissions. This activity generates a significant quantity of artificial heat sources, intensifying the heat island effect and deteriorating the quality of urban environments.

An urban heat island (UHI) occurs when a metropolis experiences significantly higher temperatures than the surrounding rural areas. The temperature differential between urban and suburban or rural areas is caused by changes in the properties of land surfaces that absorb and store heat. It slows down the rate of water evaporation in the surrounding areas, increases solar radiation absorption, and decreases convective cooling. Urban areas are experiencing rising temperatures due to the heightened utilization of resources and energy by inhabitants, leading to heightened vulnerability of the urban population to heat waves and other severe climatic occurrences.

Science has come a long way in the last 20 years in elucidating the causes of urbanization, the shifts in land use, and the consequences on city climates. Air temperature readings from ground monitoring stations or LST retrieved from thermal-infrared (TIR) remote sensing data have been used in most UHI studies. Separate temperature zones and the relationship between different logical units (LUs) are also considered. The temperature difference between urban and rural regions was previously used to produce the assessment of the UHI severity, which is thought to be the most important metric for evaluating the UHI effect. However, a limitation is the challenge of selecting temperatures that appropriately represent urban and rural locations. The distinction between urban and rural landscapes is becoming outdated due to population density, especially in India. There is no longer a clear distinction between the countryside and the city in heavily inhabited areas.

Depending on the kind of comparisons undertaken (e.g., geographical, temporal) in various studies, researchers have discovered UHI using a variety of different metrics. For instance, UHI was discovered when two time periods of an identical site were compared by measuring the variations in LST between them. This method typically compares pre- and post-urban areas' temperatures to indicate urbanization's effect on UHI. Other studies that have tracked temperature differences between urban and rural areas have also shown UHI. The outcome is a comparison of geographical units rather than two time periods. Nevertheless, the bulk of these studies are based on the actual temperatures of these places.

To calculate UHI values based on LST, researchers have recently begun using data collected from aircraft or satellites that use remote sensing. Also, this method works for tracking how land cover changes over time. The capacity to produce surface temperature data and monitor changes in land cover allowed researchers to analyze the association between changes in LULC and LST at a specific place over two periods.

The relationships between shifts in LULC and LST have been studied using several different land cover indices. NDVI, NDBI, and NDWI have been found to exhibit a strong association with LST. Worldwide, NDVI is used to map desert encroachment, monitor drought, express vegetation density, track and anticipate agricultural productivity, help identify dangerous fire zones, and express vegetation density. A dataset generated using the NDVI technique primarily represents the presence of thriving biomass. The index yields values ranging from -

1.0 to +1.0. Values close to zero mainly originate from rock and bare soil, whereas negative values primarily result from clouds, water, and snow. Lands that are dry and used for farming, consisting of rocks, sand, or snow, are associated with shallow NDVI values (0.1 and below). Parks, bushes, and meadows are characterized by moderate values ranging from 0.2 to 0.3, whereas temperate and tropical rainforests are characterized by high values ranging from 0.6 to 0.8.

The NDWI provides information about the moisture content and condition of the vegetation. Building density has an impact on NDBI. It is currently being used as an indication to show the size of built-up regions. By establishing the right threshold values, these indices are utilized to categorize various land cover types. Literature has written a lot on the connection between LST and NDVI.

The decrease in plant cover is connected to the urban thermal environment. Built-up area extraction and mapping are done using NDBI. Finding out how much water plants contain is possible with the use of NDWI analysis. Building density, land use practices, and the rate of urbanization are all closely correlated with the severity of LST. It is possible to observe the association between LULC variations and LST by arranging vegetation, water bodies, and built-up areas.

Rinner and Hussain found that LST is higher in Toronto neighborhoods with a high concentration of business and industrial properties, and they also found that NDBI and LST are correlated. Similarly, to this, Chen et al. in Guangdong Province, southern China, have demonstrated that LST has increased in prominence in places that have undergone rapid urbanization. The dynamics of heat island geographical distribution were also examined in this study. Before the UHI phenomena in the year 2000, surface temperature distributions followed a mixed pattern in 1990, with bare, semi-bare, and developed land being warmer than other surface types. In their study of the Atlanta Metropolitan Area in Georgia, Lo and Quattrochi discovered that changes in land use had a notable impact on urban heat islands (UHI) near the urban boundary.

According to research by Xiong et al., areas that are intensively industrialized, urbanized, and built up are all directly related to high-temperature anomalies. The UHI investigation of Guangzhou in South China involved the analysis of Landsat TM/ETM+ images and the examination of NDVI and NDBI indices. Xiao et al. found a high correlation between impervious surfaces and LST in Beijing, China. The correlations were analyzed using imagery obtained from Quick Bird and Landsat TM. Weng and Yang have identified that the critical factor contributing to the UHI effect in Guangzhou, China, is the presence of low-lying vegetation. LST and land cover maps were generated using Landsat TM images.

LST Variation From 2001-2021:

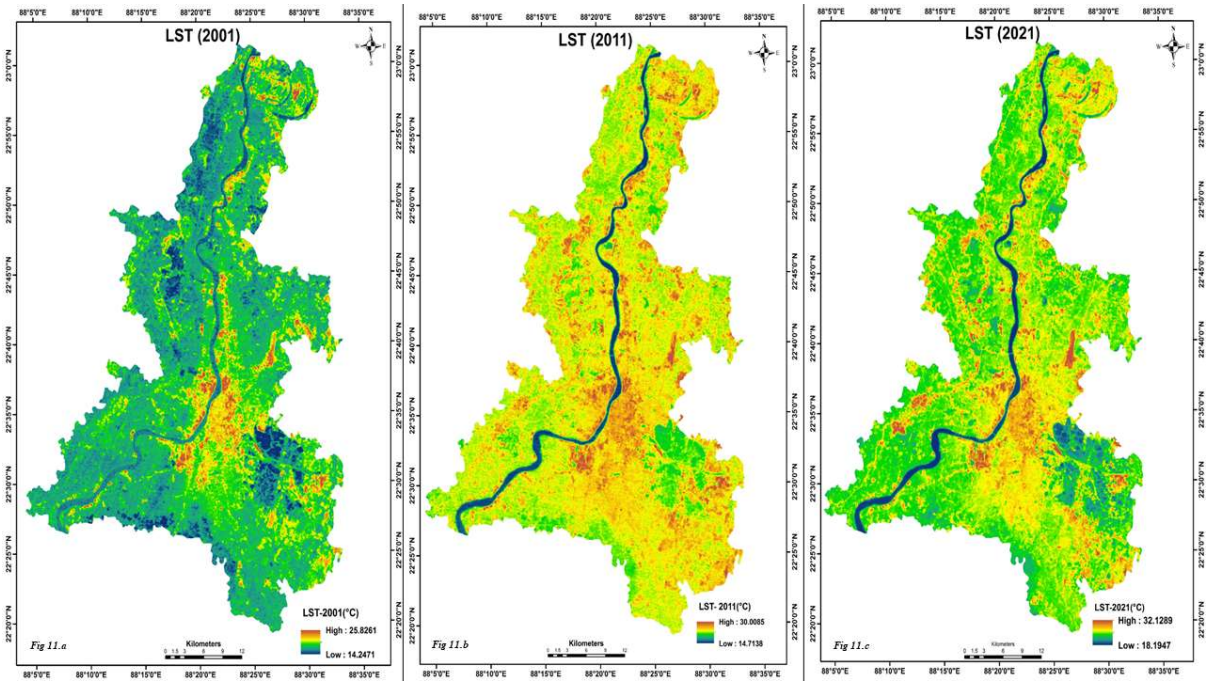

The land surface temperature (LST) was determined using the mathematical approach in equations (g-h). According to Landsat data, the mean estimated dry bulb temperature for KMC in 2001, 2011, and 2021 was 25.8°C, 29.9°C, and 31.6°C, respectively. Figure 11 (a-c) displays the value of the LST of each class for the years 2001, 2011, and 2021 at the micro-level of the analysis. In 2001, thick vegetation (17.4°C) and open space (17.9°C). The study found that surface temperature decreased as it moved towards the outer boundaries, related to the different land use patterns. Based on the investigations, the waterbody had an average surface temperature of 17.01°C and demonstrated a significant capability for heat retention and transportation. The city's central section, where most of the built-up area was located, recorded the highest temperature of 23.25°C. Numerous variables, including impervious surface, LULC, surface roughness, and building materials, had an impact on the conclusion (Aakriti & Ram, 2015). In 2001, 14.25°C was the lowest surface temperature recorded, while 25.83°C was the highest.

Class	°C	2001	2011	2021
Low	14.25-18.11	1025.844		
	14.71-19.79		157.338	
	18.19-22.57			1591.838
Moderate	18.11-21.97	752.263		
	19.79-24.87		1610.082	
	22.57-27.17			69.958
High	21.97-25.83	10.329		
	24.87-29.95		21.095	
	27.17-32.13			194.15

Table 11

According to the visual depiction and LST data for each class of land use in 2011, the surface temperature for the low temperate zone was 14.71°C to 19.8°C. The average surface temperature for the mild temperate zone ranged from 19.8°C to 24.9°C. The central part of KMC has the greatest temperature zone (24.9°C-30°C)

recorded. However, the LST value was also reported at 30°C in a few isolated areas/locations. The lowest and greatest surface temperature values for 2011 were 14.7°C and 30°C, respectively. According to Figure 10(c), the lowest temperature zone in 2021 The mean surface temperature varied within a range of 27.2°C to 28.8°C. The mean surface temperature in the mild temperature zone ranged between 28.8°C and 30.4°C. The middle portion of the research area had the highest recorded temperature (30.4°C–32°C). In the year 2021, the surface temperature ranged from a minimum of 27.2°C to a maximum of 32°C.

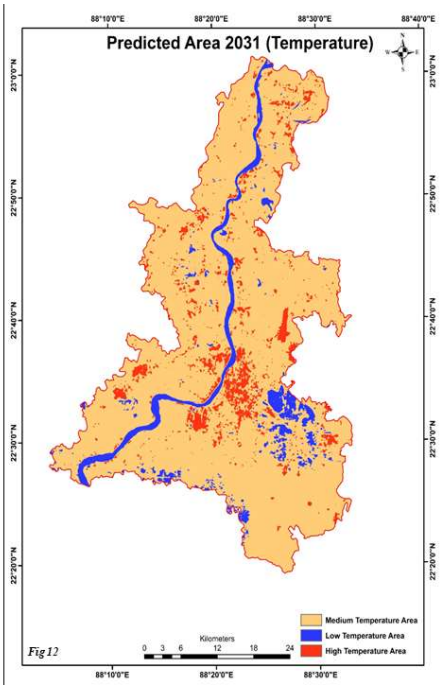

Figure 11's intersection of 2001, 2011, and 2021 LST estimates reveals an increase in surface temperature from 2001 to 2021. The natural composition of the land cover in the city is altered as a result of human activity. Therefore, LULC, surface roughness from the built-up regions, and construction materials including impermeable concrete, asphalt, and building materials led to the rise in temperature of KMC's metropolitan areas.

Model Validation:

About current land usage and the LST map from 2021, the anticipated model has been validated by 2031. The model validation tool was employed to compute Kappa values for three different scenarios: no ability (k no), standard (K standard), and location (K location). According to the data, the overall accuracy of the projected map is 0.9223 and 0.9133, which is a very excellent precise agreement. K location is 0.8795 and 0.9472, K standard is 0.8290 and 0.8672, and these values show extremely excellent agreement throughout the investigation. Making forecasts about the future is acceptable and trustworthy when the accuracy level is higher than 0.80. All Kappa index values were higher than the minimum acceptable threshold of 80%, which implies the actual and forecasted land use maps exhibit a robust concurrence, showcasing a strong agreement.

The fitting of regression equations was conducted to examine the influence of diverse spectral indices on the associated pixel LST for the years 2001, 2011, and 2021. This was done to examine the link between the spectral index and the LST, which will explain the two variables' relationship. This research utilized the LST values associated with the NDVI, MNDWI, and NDBI spectral indices obtained from the prior study. The X-axis represented the values of the spectral index, while the Y-axis represented the values of the LST. Researchers computed the R^2 values after applying the linear regression equation and analyzed them to determine the

differences among the various displays.

We explained the relationship between the LST and the land cover indices in this study. The results show that the LST is positively correlated with NDBI but negatively correlated with NDVI and MNDWI. Agricultural regions significantly influence land surface temperature in the studied area more than aquatic bodies. There is a negative correlation between the land surface temperature and both parameters. This study demonstrates the accuracy and reliability of remote sensing techniques in obtaining surface temperature data from satellite pictures. By juxtaposing the LST with the surface temperatures of the land cover, this methodology effectively diminishes the costs, workforce, and time needed to collect data on thermal patterns in vast areas. The correlation between land surface temperatures derived from Landsat satellites and land cover indicators has led to the suggestion of monitoring diverse Earth surface phenomena such as desertification, urban development and expansion, drought, and wetlands.

LST & NDVI:

Rapid urbanization has a complicated nature since it lowers the amount of greenery inside and outside cities. An abundance of beautiful green meadows has been transformed into built-up regions as a result of the population boom. As anthropogenic activity continues to worsen the natural environment in cities, Currently, the duty of monitoring alterations in land cover and urban land use falls upon policymakers, geographers, administrators, and urban planners.

According to the research, there have been considerable changes in rainfall patterns and temperature. Due to the detrimental impacts of the increasing temperature on the temporal and geographical distribution of the rainfall pattern, the groundwater aquifer is being drained. The research area's climate is influenced by the NDVI and LST. The demand-supply imbalance is made worse by these climatic changes, which also cause groundwater and surface water to become scarcer. Appiah et al. (2015), Sohail et al. (2019), Nguyen et al. (2020), and Liu et al. (2021) all found that aquifer recharge is affected by changes in rainfall patterns caused by climate change.

There is a severe threat to Earth today from the environmental issue of rising global temperatures and localized temperature swings. The land surface temperature of the Earth is controlled, in part, by environmental conditions and, in the region, by other factors (Sahani, 2021). Several types of remotely sensed data can be used to calculate urban heat using the LST. Research projects involving LST are required to apply NDVI consistently (Guha & Govil, 2020). We have extensively investigated the link between LST and vegetation using the NDVI, a reliable indicator of vegetation. Factors like LULC and urbanization affect the intricate and intriguing relationship between LST and NDVI, which scientists find intriguing (Deng et al., 2018).

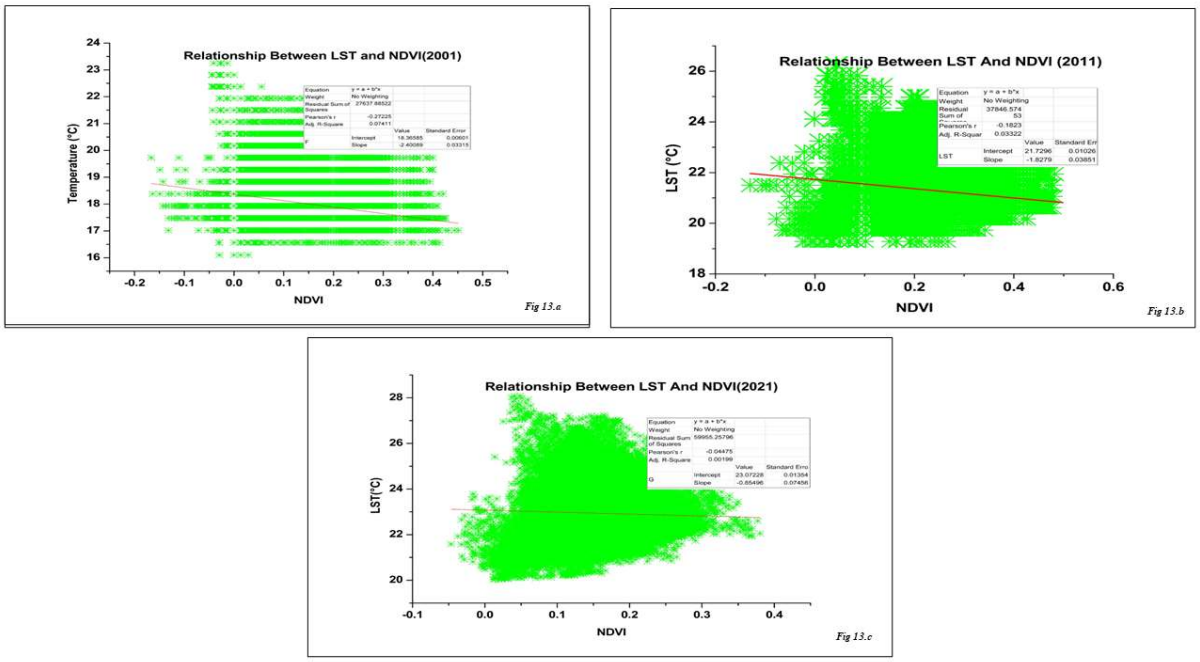

Figure 13 depicts a negative association between NDVI and LST. Because the LST values fall as the NDVI values rise, the connection is negative. For the study, the positive NDVI values above > 0.5 are utilized since they indicate the values with vegetation. For all the years of analysis in the research period, the R2 values for the correlation between NDVI and LST are above -0.3, indicating a good association. Because of the reduction in vegetative areas throughout the research period, the mean LST has risen. Temperature changes are significantly influenced by the plant cover. According to the graph, between 2001 and 2021, the vegetation cover decreased, which increased LST.

LST & MNDWI:

Urban land use planning and development heavily relies on LST-related studies (Li et al. 2017). Within urban environments, the terms "urban heat island" and "urban hot spots" are frequently used to describe the specific locations within cities with significantly elevated LST (Guha et al., 2017). The NDWI is the most commonly used method for extracting water surface information. It is frequently utilized in LULC research and LST analysis. Several studies have employed this index, including those by McFeeters (1996), Chen et al. (2006), Essa et al. (2012), Yuan et al. (2015), and Guha et al. (2020b). Humidity, vegetation, wetlands, bare ground, air pollution, rock surface, dry or wet soil, and various artificial materials are some of the criteria used to determine how insignificant the relationship between LST and NDWI is in an urban setting (McFeeters, 1996; Ghobadi et al., 2014; Guha et al., 2020c).

A weak correlation between NDWI and LST was found when the entire Wuhan City, China, metropolitan area was considered (Wu et al., 2019). According to Choudhury et al. (2019), India's Asansol-Durgapur Development Region water bodies negatively correlate with the connection between LST and NDWI. The bodies of water in Nanchang City, China, were discovered by Zhang et al. (2017) to be negatively correlated with LST and NDWI. The opposite is true in Shenzhen City, where a strong negative association was discovered between LST and NDWI about bodies of water (Chen et al., 2006).

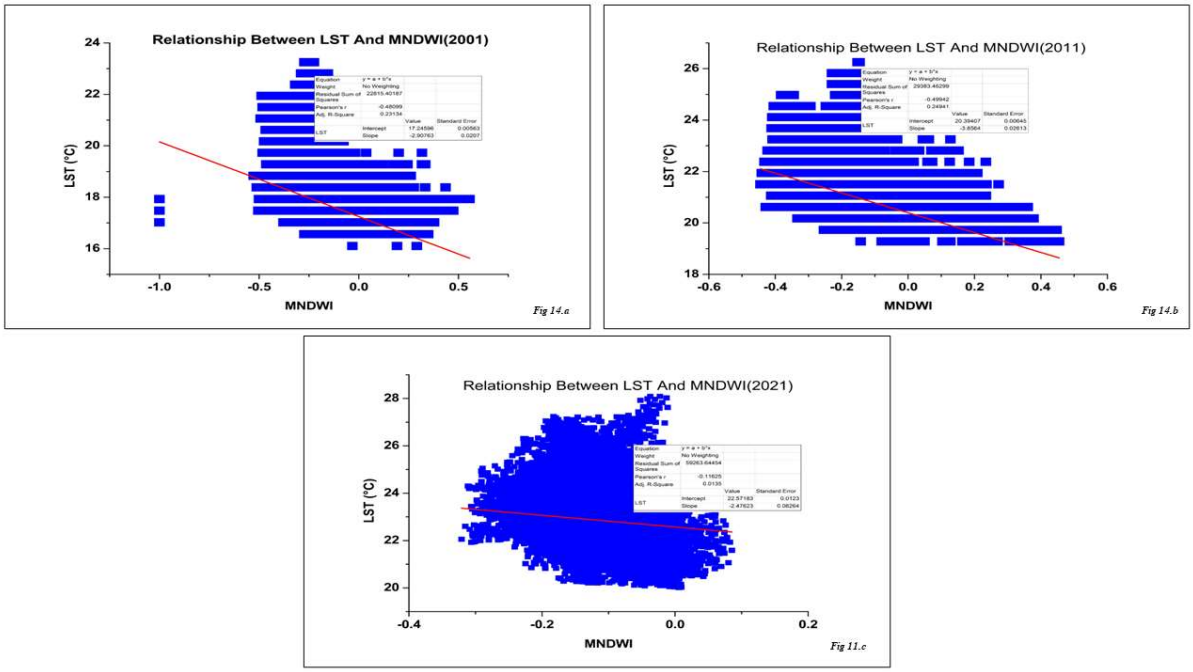

Figure 14 There is an inverse correlation observed between MNDWI and LST. Because the LST values are falling while the MNDWI values are rising, the relationship is negative. Since it represents values with water pixels, the study uses the positive value of MNDWI above 0. The association between MNDWI and LST has R^2 values over -0.1, which indicates a strong connection. Because the LST values fall as the MNDWI values rise, the relationship is negative. Due to a reduction in the quantity of LULC in aquatic bodies, the mean LST increased during the course of the research. The local climate of the region is significantly influenced by the water bodies there. Between 2001 and 2011, the water body shrank as the LST rose. Since the typical values are below 25 °C, the water bodies have the greatest impact on LST. The MNDWI and LST have a negative association, with in 2021, there was a modest correlation coefficient of -0.12, whereas, in 2001, a stronger correlation coefficient of -0.49 was observed. The MNDWI pixel values surrounding the samples in KMC were much lower in 2021 as a result of the previous year's lack of rainfall.

LST & NDBI:

The NDBI is crucial in assessing and measuring the LST (Grover and Singh 2015). Xiong, Huang, Chen, Ye, Wang, and Zhu (2012) found a direct correlation between high-temperature anomalies and places with built-up land, densely inhabited regions, and extensively industrialized districts. According to Chen, Zhao, Li, and Yin (2006), NDBI exhibits sensitivity towards developed areas, with its values ranging from -1 to +1. Positive values indicate extensively developed land, whereas negative values represent various types of land cover. For estimating NDBI, equation (e-f) is used (Chen et al., 2006; Xu, 2008). Figure 14 depicts The NDBI classifications derived for 2001, 2011, and 2021, illustrating the size and distribution of urbanized and non-porous land regions. The NDBI values ranged from -0.4 to +0.4, respectively. However, relatively high NDBI values were found across the city, particularly in the central region, except the areas around water bodies.

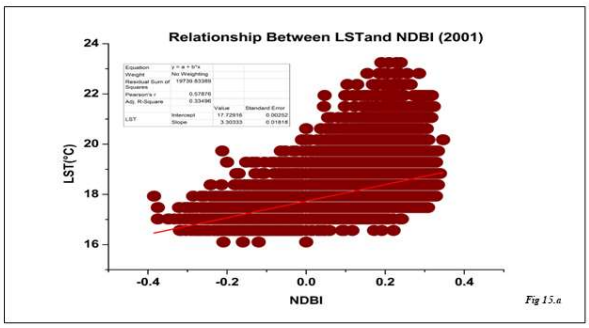

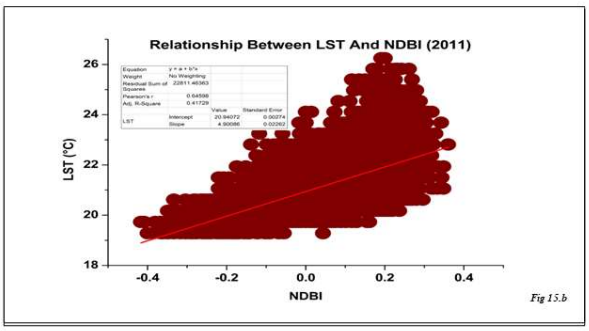

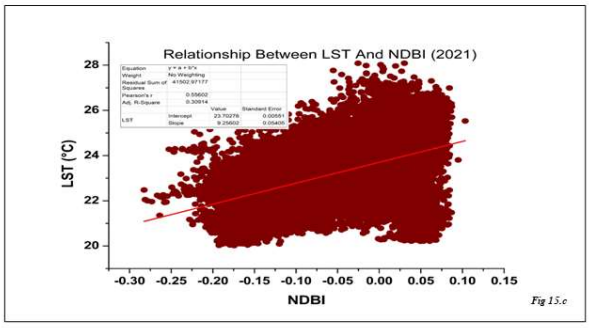

For the study, the positive NDBI values over 0 are used as they primarily reflect the built-up area. After investigating their interactions, a clear link between NDBI and LST was identified. According to the NDBI results, the built-up regions exhibited the highest surface temperature. So, it was expected that urbanization or built-up regions would result in notable differences in surface temperature. Figure 15 demonstrates a notable positive correlation between the NDBI and LST. For all of the years of analysis throughout the research period, the correlation between NDBI and LST exhibits a robust association, as evidenced by R2 values exceeding 0.60. Due to the growing built-up area throughout the research period, the mean LST rises. LST patterns may vary as a result of LULC changes, particularly urban growth (Weng 2001; Xiao & Weng 2007). The graph demonstrates that when the LST climbed between 2001 and 2021, the built-up area expanded dramatically as well.

LST and Hotspot:

Several investigations have been conducted to pinpoint LST hotspots or areas characterized by elevated LST values and exceptionally intense heat stress. (Chen et al. 2006; Ren et al. 2013; Feyisa et al. 2016; Lopez et al. 2017; Guha et al. 2017; Tran et al. 2017; Pearsall, 2017; Sharma et al. 2022). Identification of LST hotspots is important for mitigation efforts and for preserving a city's ecological balance. Using the Getis Ord Gi* statistics clustering approach, Tran et al. (2017) identified LST hotspots.

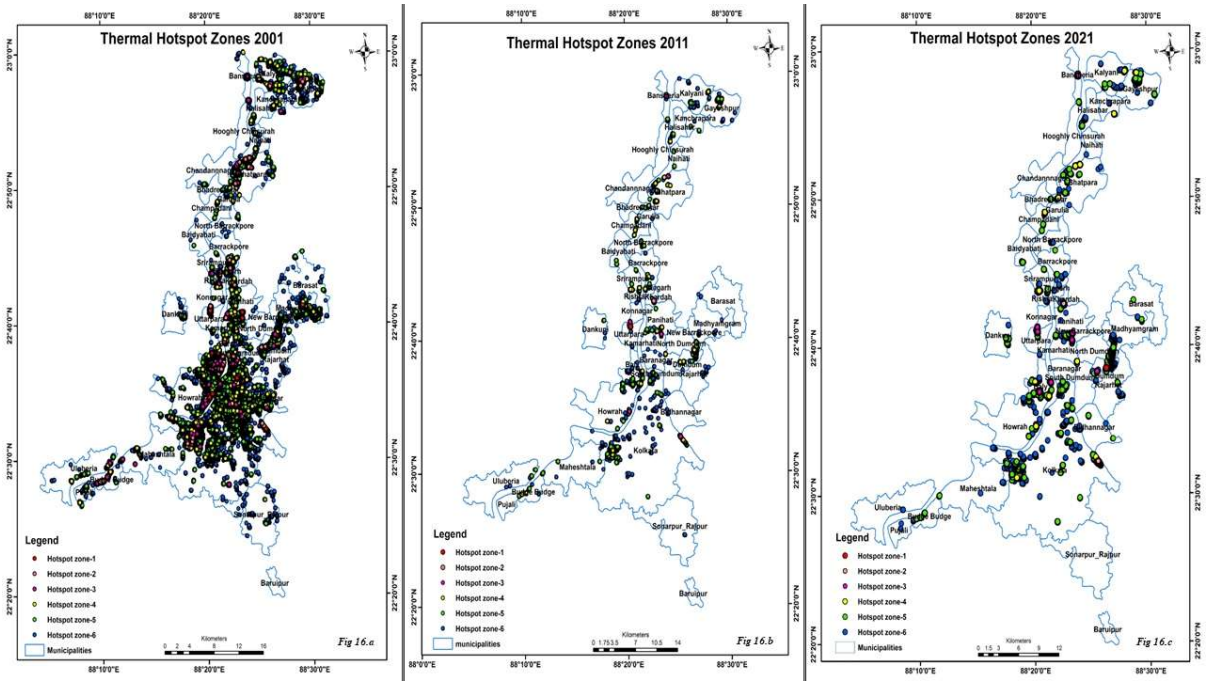

To identify areas with high LST values (hot spots) and areas with low LST values (cold spots) in the studied area, the Getis Ord GI* statistic was applied. The concentration of high values (hot spot) is more apparent when the z-score is significantly positive. On the other hand, a smaller negative z-score indicates that more concentrated groups of values are shared (cold place). For an area to be classified as a hot spot, it must have many high LST readings; a single higher LST measurement must be revised. To better understand temporal LST patterns, the Gi statistic provides a more holistic view than looking at very high or low values. The current investigation considered hot and cold spots with a confidence level higher than 95%. According to Maithani, Nautiyal, and Sharma (2020), the GI* statistic is thoroughly covered in ESRI (2016).

In our study region, we are analyzing the temporal changes of LST over the 20 years, and analyzing the LST hotspot zone by using a random sampling method, whereas in each year we plotted random 2000 points. Table 12 indicates the hotspot zones of 2001, 2011, and 2021.

Thermal Hotspot Zone	2001	2011	2021
Zone 1	20.17-20.83	25.40-26.17	27.00-27.85
Zone 2	20.83-21.49	26.17-26.94	27.85-28.71
Zone 3	21.49-22.14	26.94-27.70	28.71-29.56
Zone 4	22.14-22.80	27.70-28.47	29.56-30.42
Zone 5	22.80-23.46	28.47-29.24	30.42-31.27
Zone 6	23.46-24.11	29.24-30.00	31.27-32.13

Table 12

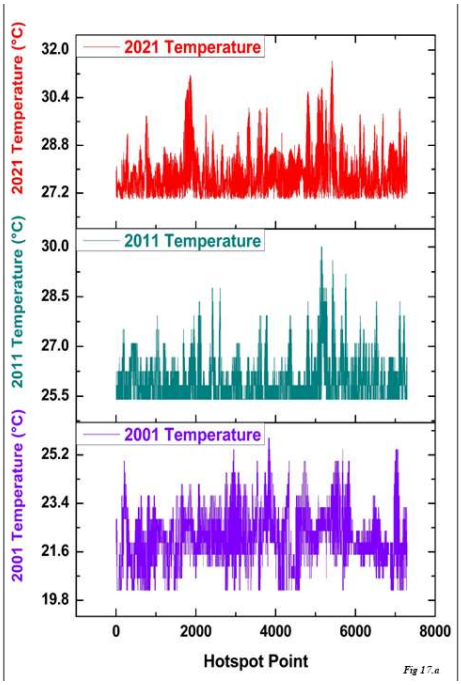

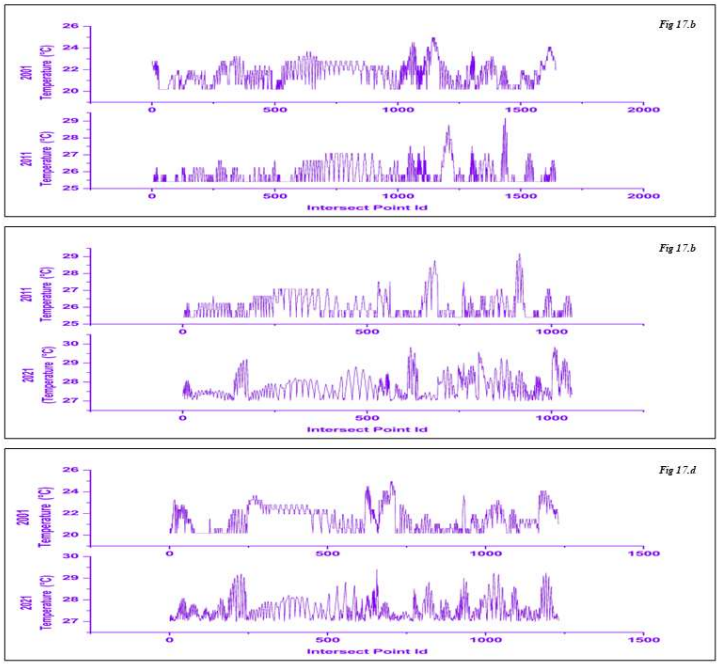

The urbanization process has led to a rise in the proportion of developed land, increasing in built-up areas. In contrast to the uniform pixels that once made up non-built-up land cover classes, these regions with a more diverse composition display increased LST values. As a result, there is a more robust accumulation of higher LST readings in urban areas compared to previous years. The increased concentration of developed regions in places with high temperatures can be linked to the urban design, which decreases the amount of open sky and restricts the process of evaporation, together with the influence of human-made heat sources. In 2001, The hotspots were concentrated in the southern and central parts of the municipal territory, resulting in a smaller overall area of habitation. The densification and extension of hotspot areas occurred in 2011. According to the 2021 results, hotspots shifted to the western and northern parts of the municipal territory. The southern and western portions of the municipal jurisdiction have very few hotspots. All three years, the municipal area's center continued to be a hotspot. (Figure 17).

UHI Extent from City Centre Outwards:

Urbanization is an unstoppable phenomenon that cannot be controlled or stopped, but it may be managed sustainably through integrated land use planning. According to Cobbinah and Clifford (2012) and Sharma and Joshi (2013), Urban growth is the term used to describe the enlargement of the developed region, signifying the migration of individuals from the central urban zone to the peri-urban areas located on the outskirts of the city. This unplanned urban growth harms the environment, leading to local and regional socio-ecological system alterations. The negative impacts include the loss of productive farmland, fragmentation of wildlife habitats, elevated city temperatures, and reduced biodiversity (Maithani, 2009; Kumar and Pandey, 2016; Pawe and Saika, 2017; Kar et al., 2018).

The main contributors to urban heat islands are haphazard, unplanned urbanization and subpar building design. Research indicates that in urban areas, the built environment has undergone a transformation where natural spaces have been substituted with impermeable and scorching surfaces composed of concrete and asphalt, which is the main culprit for UHI. The heat from the sun is more effectively absorbed by these surfaces than it is reflected, increasing both the surface temperature and the ambient temperature. The air trapped between tall buildings and narrow streets can also be heated. The UHI effect is influenced by various factors, including urban geometry (such as the dimensions, configuration, elevation, and organization of buildings), the thermal

characteristics of urban surfaces, the scarcity of greenery, the widespread reliance on air conditioning in hot climates, industrial activities, automobile usage, and the extent of urban development within a city. Due to the reduced moisture content in the urbanized areas of a city, including the roofs, walls of buildings, roads, parking lots, industrial zones, and commercial areas, the evaporation of water into the atmosphere is minimized. Consequently, this leads to elevated surface and air temperatures. However, urban greenery acts as a natural cooling mechanism, which is the exact opposite.

The multiple-ring buffer (Figure 15a) analysis employed in this study does the urban area's diverse components justice. This model is a mix of factors, including LST data and its temporal variation as well as a three-year growth rate based on the reference year. The many rings are produced equally far from the city hub. The ring buffer offers a variety of LST classes that are evenly spaced from the city core and provide a quick overview of the dispersion of temporal temperature changes. The fundamental reasons for the LST decline tendency and their distributional characteristics are satisfied by this data.

The LULC data categorization and their temporal change in land use about growth were used in this model. These many rings are produced using the city's core (the junction of the North, South, and East-West profiles), spaced 10 km from the source. Using ArcGIS software, a total of 26 buffer zones were created for the years 2001, 2011, and 2021.

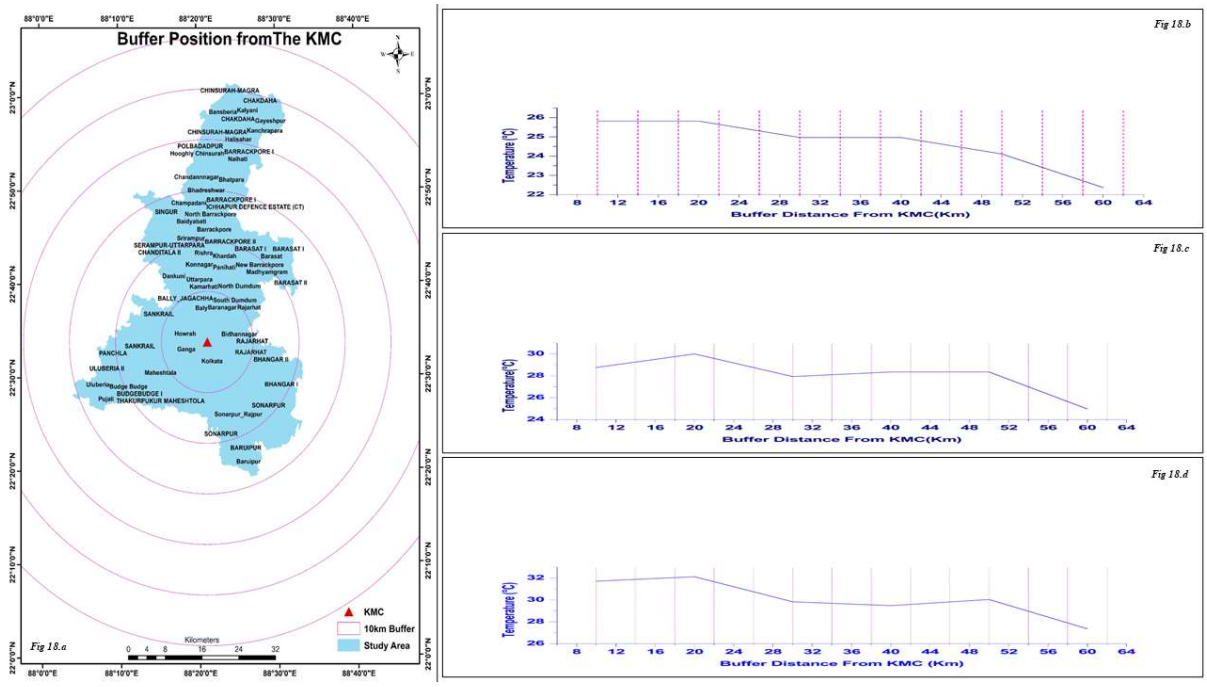

Figure 18(b-d) in this analysis shows the variations in urban density and the LST reduction from the city center outward. A noticeable decrease in Land Surface Temperature (LST) can be observed every 10 km away from the central area. A comparison analysis was carried out using the Land Surface Temperature Maps to provide a comprehensive understanding of the urban heat island phenomenon in the study area (Sen and Bhattacharjee, 2021). A phenomenon known as urban heat island occurs when urban regions endure higher temperatures than their rural equivalents. The rise in the urban heat island effect is mainly attributable to the rising concretization and urbanization, as much of the emitted terrestrial radiation is trapped within buildings and concreted roads. Because of this, the temperature range in cities is becoming wider. Furthermore, the open ground absorbs a large portion of the heat that causes the urban heat island effect.

Over time, the land use patterns in the research region have changed in specific ways, leading to the creation of

UHI. It is widely acknowledged that urbanization is predominantly responsible for the formation of urban heat islands. The masonry constructions, such as buildings, paved streets, skyscrapers, etc. absorb a lot of heat to trap it. An urban heat island is created when this stored energy causes the temperature in an urban environment to increase faster than it does in rural settings. The urban heat island phenomenon has been linked to the consistent high temperatures observed in the research region over the years. The built-up area coverage of the research region witnessed a consistent increase in the years 2001, 2011, and 2021. About 18% of the study region's total area was covered by buildings in 2001; this number rose to 23% in 2011; and it will skyrocket to 30.43% in 2021. The continuous expansion of built-up areas in the KMC can be attributed to the extensive transformation of both barren lands and densely vegetated regions into urbanized spaces. A large section of the study region is also unproductive land, which is believed to have contributed to the development of the urban heat island phenomenon over time, even though it shows a decreasing tendency (Macarof and Florian, 2017). This is because arid ground absorbs between 70 and 80 percent of incoming solar light. Urban heat island is also believed to have increased through time as a result of a decline in the area covered by thick vegetation. This is because plants and trees in rural regions provide shade and reduce the temperature through evapotranspiration.

LST difference in Rural-Urban Fringe Areas:

Luke Howard first introduced the idea of UHI in 1833, and since then, the study on the subject has progressively been more in-depth. UHI is an urban region that is much warmer than the nearby rural areas in a larger geographic context. On the other side, a UHI can also happen inside a city region, meaning that one sector of the city is much hotter than the other parts. When compared to daylight, summer, and heavier wind conditions, the temperature differential is often greater at night, in winter, and when there is less wind. However, based on the Spatiotemporal context of an investigation, an alternative outcome can also be possible.

Ohashi and Kida (2002) It has been proven that in conditions of clear skies and minimal wind, urban areas tend to be approximately 10 °C warmer than the surrounding rural regions. Souch and Grimmond (2006) have said that the UHI phenomenon is primarily noticed at night but can occur at any time of the year, contingent upon factors such as wind patterns. Urban and commercial locations typically exhibit elevated temperatures, whereas residential and rural regions typically display lower temperatures.

The correlation between population, primary natural resources, urbanization, and the natural environment is indisputable. The expansion of economies and industries and people moving from rural to urban regions are only a few factors that have caused significant changes in cities and metropolitan areas worldwide (Shirazi & Kazmi, 2014). Several factors encourage urban expansion, such as replacing natural land covers with non-permeable urban materials, which disrupts the land surface's energy development and negatively impacts the land's features (Bongaarts, 2006). Population growth is a significant factor in this situation.

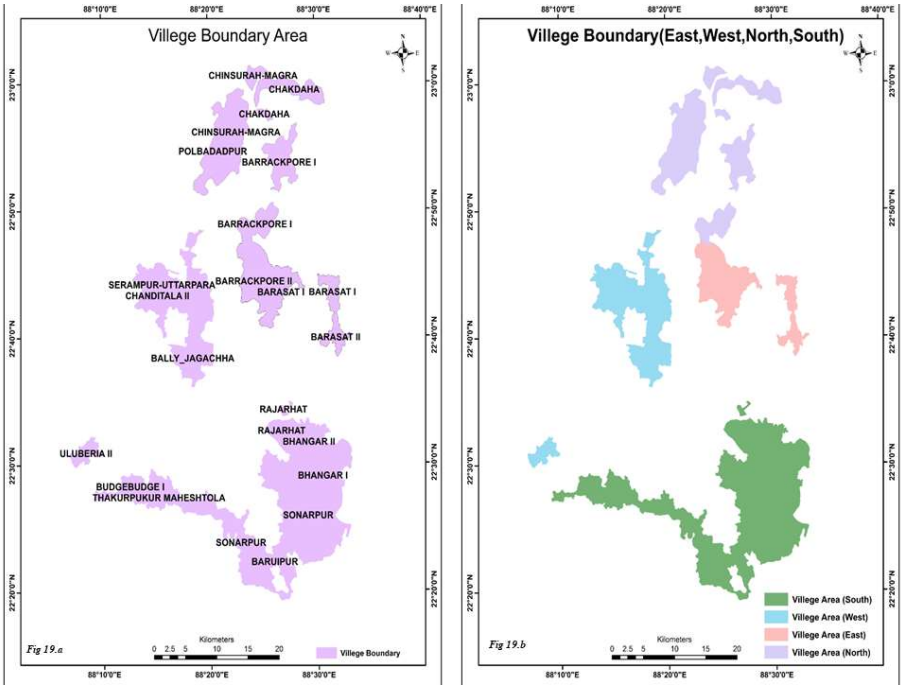

In both rural and urban parts of KMC, we examined the land surface temperature (LST) for different land use/cover types using the LST and LULC maps. This analysis is depicted in Figure 19 a-b. The primary land-use elements, including urbanized spaces, undeveloped land, unused land, agricultural land, residential vegetation, and bodies of water, displayed noticeable differences in land surface temperatures (LSTs) between urban and rural sites. The LSTs followed a decreasing order, with the highest mean LST of 27.69˚ C observed in urban and rural residential regions. These regions were characterized by a significant presence of built-up areas, which constituted a substantial proportion of the land usage. The average land surface temperature (LST) in urbanized regions was approximately 2˚ C higher compared to the agricultural land, predominantly located near rural residential zones. Homestead LSTs exhibited a slightly higher value than vegetation LSTs. The lower LSTs were predominantly observed in places outside of the KMC (Kolkata Municipal Corporation) and exhibited an approximate decrease of 8˚C compared to LSTs within urbanized regions. The levels of LSTs were at their minimum in the vicinity of water bodies. The LSTs in the KMC neighborhoods were lower compared to the rural eastern and southern regions.

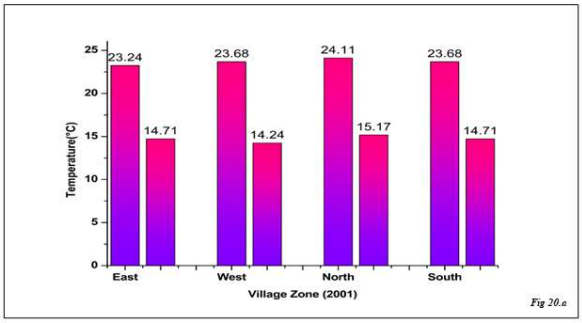

Fig 20.a

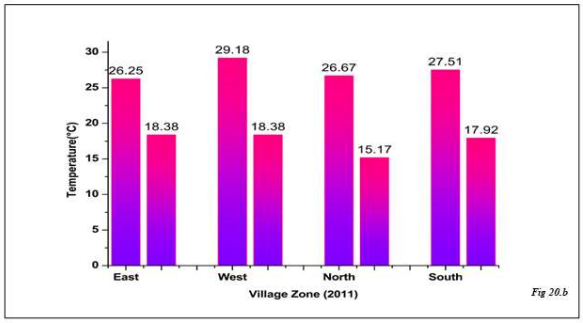

Fig 20.b

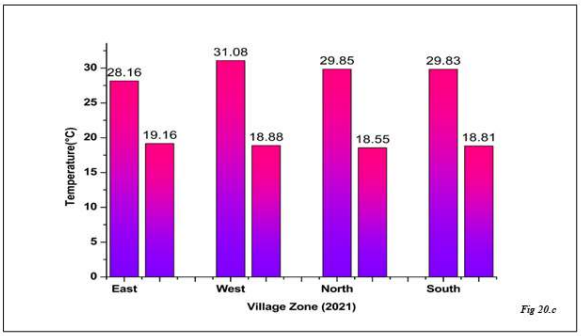

Fig 20.c

There is a distinct temperature variation represented in Figure 19(a-c) of each village zone in every study year. In the year 2001, the northern part of the villages had the highest temperature reach is more than 24˚ C and the villages under the western zone had a minimum temperature is less than 15˚ C. Southern and Eastern parts of villages had almost the same temperature variation of maximum 24˚ C and minimum 15˚C, whereas northern villages facing a highest minimum of more than 15˚ C.

Phase 2 saw scientists notice an increase in temperature in four localized regions of the town due to land use and cover changes. The changes include expansion of residential areas, transformation of farmland, and clearing of forested areas to make way for new fields. In this time frame, the western zone has the highest maximum temperature rise is less than 30˚ C, on the other side the northern part faces the lowest maximum temperature is 15˚ C. In this period, we also noticed that northern villages comparatively face lower temperatures whereas eastern and southern villages have moderate temperature rises.

In the third phase, the temperature rise is maximized in the study villages. Due to the urbanization taking place in the western part of the KMC, this region faces maximum and minimum temperature rise than the other three zones. The overall temperature rises in every village zone, western villages take the first place followed by northern, southern, and eastern villages. In this time frame the maximum temperature reach in village areas was more than 31˚ C and the minimum temperature reach was 18˚ C.

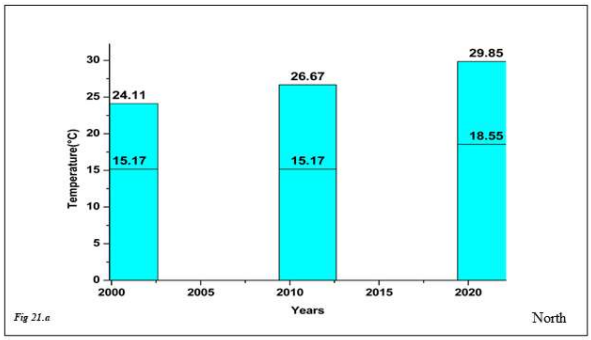

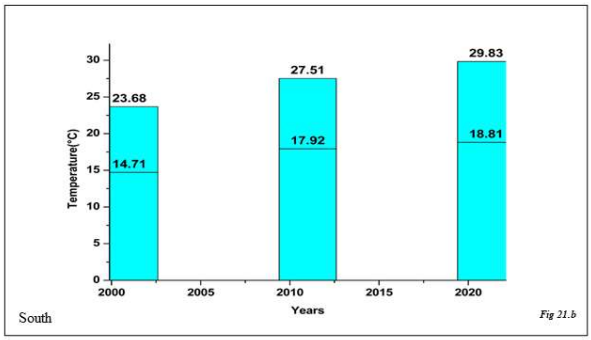

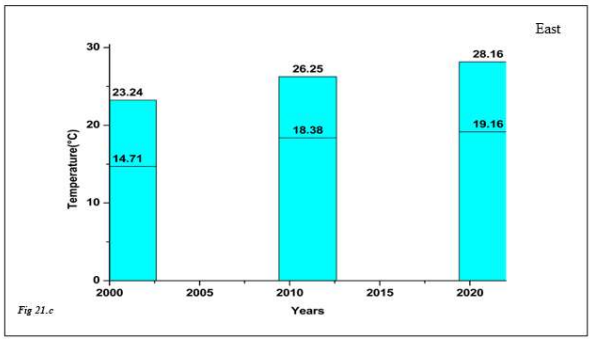

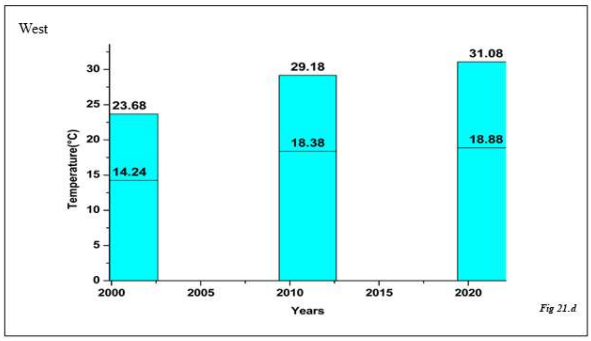

In this comparative analysis, the temperature change has been observed (Figure 20 a-d) every ten years of the referenced year. The Northern Region, in 2001 and 2011 had the same minimum temperature of 15.17˚ C but in 2001 the maximum temperature was 24.11 and it rose nearly 2˚ c in between 2011 reaching 26.67. In 2021 remarkable changes were observed nearly 3˚ C of temperature rose in each case the minimum temperature was 18.55 and the maximum was 29.85. The Eastern Region, in 2001 faced a minimum temperature of 14.71 and a maximum was 23.24, and in 2011 had a 4˚ Crise in temperature so the minimum temperature was 18.38˚ C but, in the 3,˚C rise, the maximum temperature was 26.25. In 2021 temperature rise gets slow like maximum temperature reaches only 1˚C high (19.16), and 2˚C high in maximum temperature is 28.16.

The Southern and Western Region, in 2001 faced a minimum temperature of 14.71 and 14.24 respectively and the maximum was 23.68 in each region. In the next phase (2011) it had only a 3˚ C, and 4˚ C rise in temperature so the minimum temperature of the southern region and western region of the study area was getting of 17.92 and 18.38, whereas, the maximum temperature of the southern region rise 4˚ C and now it reaches 27.51, and in the western region it takes place 6˚ C rise now it reaches 29.18. In the last phase (2021), the temperature-increasing tendency gets low, the southern and western regions having minimum temperature rose nearly 1˚C, so it reaches 18.81 and 18.88 respectively and maximum temperature having 2˚ C rise so it reaches 29.83 and 31.08 accordingly.

Conclusion:

Comprehending the changes over time in the arrangement of land cover and the growth of urban areas is essential for efficient land administration and the development of sustainable urban plans. This study used photos taken at different times to show how LULC has changed and how the Kolkata Metropolitan Development Authority (KMDA) in West Bengal plans to grow cities. Up to 2021, it was a part of the study. Afterward, we used a CA-Markov model that was incorporated to predict when things would change. The inquiry started by looking at how cities were growing, how farmland was shrinking, how residential areas and forest cover were barely changing, how bodies of water and abandoned land were changing, and how wetland zones varied slightly. After 2001, there was fast urbanization and the loss of agriculturally productive land. To showcase the spatial and temporal progression of urban growth starting from the city center and expanding outward, our subsequent analysis focused on examining the direction and extent of urban expansion through ring-based

analysis. The district as a whole has not seen urban growth at the same rate. Previously agricultural property near road networks and in locations with easy access from the urban centre has seen higher levels of urbanization. The East-West axis had the highest concentration of urbanization.

The fast growth of metropolitan areas is causing the loss of vital agricultural land, leading to food insecurity and environmental damage. This trend is anticipated to persist and worsen in the future. Developing and implementing comprehensive urban planning strategies is paramount to safeguard highly productive agricultural land. Creating a resilient urban environment and promoting sustainable growth depends on careful urban planning that protects agriculture, green spaces, and open places. The government's main goal should be to implement proactive measures that deter mass immigration by employing diverse migration controls and redirection strategies. We suggest utilizing the CA-Markov model as a suitable instrument for future investigations into the intricate configuration of urban and land use/land cover. Ultimately, urban planners, politicians, and other experts should see our findings as a noteworthy milestone.

Sunlight, air pressure, and land surface features all had a role in the LST's dramatic swings throughout the urban-rural spectrum. The analysis of LSTs' geographical and temporal features about land-cover types, land-use categories, and urban structure was made more accessible by integrating ground-based observations and remotely sensed data. Significantly, there were substantial disparities in LST between urban and rural areas, with urban regions exhibiting LSTs roughly 3-6˚ C higher than their rural counterparts. Furthermore, in metropolitan areas, there were notable disparities in land-use types, including impervious surfaces, green spaces, and water, which resulted in considerable changes in LST. LSTs near impervious surfaces were found to be 6-12°C higher than those near green spaces. The results of our study suggest that variations in land surface radiation and energy fluxes mainly caused differences in land surface temperatures in urban areas. The most significant contributor to net radiation for impermeable surfaces was sensible heat flow, leading to increased LST. On the other hand, the predominant source of net radiation for green spaces was latent heat flux.

The configuration of metropolitan areas, the choice of construction materials in cities, and the altitude and vegetation coverage in rural areas significantly influence LST. It was noted that as the MNDWI and NDVI both increased, LST decreased. City planners and designers must prioritize selecting appropriate construction materials, organizing urban structures logically, increasing the number of green spaces, and creating cohesive landscape components. Implementing these steps is essential for reducing the severity of the UHI phenomenon in KMC.

References:

1. Bhatta B (2009) Analysis of urban growth pattern using remote sensing and GIS: a case study of Kolkata, India. Int J Remote Sens 30(18):4733–4746
2. Mukherjee M (2012) Urban growth and spatial transformation of Kolkata metropolis: a continuation of colonial legacy. ARPN J Sci Technol 2:365–380
3. Roy D, Lees M, Palavalli B, Pfeffer K, Sloot M (2014) The emergence of slums: a contemporary view on simulation models. Environ Model Softw 59:76–90
4. Sugiyama M (2008) The study on climate impact adaptation and mitigation in Asian coastal megacities integrated research system for sustainability science. University of Tokyo. Final Report to JICA
5. Ghosh D, Sen S (1987) Ecological history of Calcutta's wetland conversion. Environ Conserv 14 (3):219–226
6. Dasgupta S, Asvani K, Gosain K, Rao S, Roy S, SarrafM(2013) A megacity in a changing climate: the case of Kolkata. Clim Chang 116:747–766
7. Zeng, Q., Xie, Y., Liu, K., 2019. Assessment of the patterns of urban land covers and impervious surface areas: A case study of Shenzhen, China. Phys. Chem. Earth. 110,1–7.

8. Seto, K.C., Güneralp, B., Hutyra, L.R., 2012. Global forecasts of urban expansion to 2030 and direct impacts on biodiversity and carbon pools. Proc. Natl. Acad. Sci. 109 (40), 16083–16088.
9. Reed, M.S., Kenter, J., Bonn, A., Broad, K., Burt, T.P., Fazey, I.R., Stringer, L.C., 2013. Participatory scenario development for environmental management: a methodological framework illustrated with experience from the UK uplands. J. Environ. Manage. 128, 345–362.
10. Ghosh, S., Chatterjee, N.D., Dinda, S., 2019. Relation between urban biophysical composition and dynamics of land surface temperature in the Kolkata metropolitan area: a GIS and statistical-based analysis for sustainable planning. Model. Earth Syst. Environ. 5 (1), 307–329.
11. Nuissl, H., Haase, D., Lanzendorf, M., Wittmer, H., 2009. Environmental impact assessment of urban land use transitions—a context-sensitive approach. Land Use Policy 26 (2), 414–424.
12. Jenks, M.J., Burgess, M.J.R., Acioly, C., Allen, A., Barter, P.A., Brand, P., 2000. Compact Cities: Sustainable Urban Forms for Developing Countries. Taylor & Francis.
13. Turner II B L, Skole D, Sanderson S, Fischer G, Fresco L and Leemans R 1995 Land use land cover change science/research plan (IGBP Report No. 35 and HDP Report No. 7).
14. Mather J R and Sdasyuk G V 1991 Global change: Geographical approaches (Tucson Arizona USA: University of Arizona Press).
15. Thomas H and Laurence H M 2006 Modeling and projecting land-use and land-cover changes with a cellular automaton in considering landscape trajectories: An improvement for simulation of plausible future states; EARSeL eProc. 5 63–76.
16. Boerner R E J, Demers M N, Simpson J W, Artigas F J, Silva A. and Berns L A. 1996 Markov models of inertia and dynamic on two contiguous Ohio landscapes; Geogr. Anal. 28 56–66.
17. Torrens, PM., O'Sullivan, D. (2001). Cellular automata and urban simulation: where do we go from here? Environment and Planning B: Planning and Design, 28, 163-168
18. Jokar Arsanjani J, Helbich M, Kainz W, Bloorani A D 2013b Integration of logistic regression, Markov chain, and cellular automata models to simulate urban expansion. International Journal of Applied Earth Observations and Geoinformation 21: 265–75.
19. Shafizadeh Moghadam, H., Helbich, M. (2013). Spatiotemporal urbanization processes in the megacity of Mumbai, India: a Markov chains-cellular automata urban growth model, Appl. Geogr., 40, 140-149
20. Celik, B., Kaya, Ş., Alganci, U., Seker, DZ. (2019). Assessment of the relationship between land use/cover changes and land surface temperatures: a case study of thermal remote sensing, FEB Fresenius Environ. Bull.,3, 541
21. Pontius Jr, R. G., Huffaker, D., Denman, K. (2004). Useful techniques of validation for spatially explicit land-change models. Ecological modeling, 179(4), 445-461.
22. Kamusoko C, Aniya M, Adi B, Manjoro M (2009) Rural sustainability under threat in Zimbabwe–simulation of future land use/cover changes in the Bindura District based on the markov-cellular automata model. Appl Geogr 29(3):435–447
23. Clarke, K. C., Hoppen, S., Gaydos, L. (1997). A self-modifying cellular automaton model of historical urbanization in the San Francisco Bay area. Environment and Planning B: Planning and design, 24(2), 247-261.
24. Department of Economic and Social Affairs, Population Division. (2015). World Urbanization Prospects: The 2014 Revision (ST/ESA/SER.A/366). United Nations, New York.
25. Lin, C., Li, Y., Yuan, Z., Lau, A.K.H., Li, C., Fing, J.C.H. (2015). Using satellite remote sensing data to estimate the high-resolution distribution of ground-level PM 2.5. Remote Sensing of Environment, 156, 117-128.
26. NRC (U.S. Nuclear Regulatory Commission). (1999). Environmental Standard Review Plans for Environmental Reviews for Nuclear Power Plants (NUREG-1555). Washington, D.C.
27. Lambin, E.F., Rounsevell, M.D.A., Geist, H.J. (2000). Are agricultural land-use models able to predict changes in land-use intensity? Agriculture, Ecosystems & Environment, 82(1-3), 321-331.

28. Wang, S.W., Munkhnasan, L., Lee, W.K. (2021). Land use and land cover change detection and prediction in Bhutan's high-altitude city of Thimphu, using cellular automata and Markov chain. Environmental Challenges, 2, 100017.
29. Jat, M.K., Choudhary, M., Saxena, A. (2017). Application of geospatial techniques and cellular automata for modeling urban growth of a heterogeneous urban fringe. The Egyptian Journal of Remote Sensing and Space Science, 20(2), 223-241.
30. Li, X., Yeh, A.G. (2002). Neural-network-based cellular automata for simulating multiple land use changes using GIS. International Journal of Geographical Information Science, 16(4), 323-343.
31. Hathout, S. (2002). The use of GIS for monitoring and predicting urban growth in East and West St Paul, Winnipeg, Manitoba, Canada. Journal of Environmental Management, 66(3), 229-238.
32. Maithani, S. (2010). Application of Cellular Automata and GIS Techniques in Urban Growth Modelling: A New Perspective. Institute of Town Planners, 7(1), 36-49.
33. Sangermano, F., Eastman, J.R., Zhu, H. (2010). Similarity Weighted Instance-based Learning for the Generation of Transition Potentials in Land Use Change Modeling. Transactions in GIS, 14(5), 569-580.
34. Bununu, Y.A. (2017). Integration of Markov chain analysis and similarity-weighted instance-based machine learning algorithm (SimWeight) to simulate urban expansion. International Journal of Urban Sciences, 21(2), 217-237.
35. Zubair, O.A., Ji, W., Weilert, T.E. (2017). Modeling the Impact of Urban Landscape Change on Urban Wetlands Using Similarity Weighted Instance-Based Machine Learning and Markov Model. Sustainability, 9(12), 2223.
36. Mandal, J., Ghosh, N., Mukhopadhyay, A. (2019). Urban Growth Dynamics and Changing Land-Use Land-Cover of Megacity Kolkata and Its Environs. J Indian Soc Remote Sens, 47, 1707–1725.
37. Jokar Arsanjani, J., Helbich, M., Keinz, W., Boloorani, A.D. (2013). Integration of logistic regression, Markov chain, and cellular automata models to simulate urban expansion. International Journal of Applied Earth Observation and Geoinformation, 21, 265-275.
38. Shafizadeh Moghadam, H., Helbich, M. (2013). Spatiotemporal urbanization processes in the megacity of Mumbai, India: A Markov chains-cellular automata urban growth model. Applied Geography, 40, 140-149.
39. Guan, D., Li, H., Inohae, T., Su, W., Nagaie, T., Hokao, K. (2011). Modeling urban land use change by the integration of cellular automaton and Markov model. Ecological Modelling, 20-22, 3761-3772.
40. Celik, B., Kaya, S., Alganci, U., Seker, D.Z. (2019). Assessment of the relationship between land use/cover changes and land surface temperatures: a case study of thermal remote sensing. Fresenius Environmental Bulletin, 28 (2), 541-547.
41. Sekertekin, A., Kutoglu, S.H., Kaya, S. (2016). Evaluation of spatio-temporal variability in Land Surface Temperature: A case study of Zonguldak, Turkey. Environ Monit Assess, 188, 30.
42. Pontius Jr., R.G., Huffaker, D., Denman, K. (2004a). Useful techniques of validation for spatially explicit land-change models. Ecological Modelling, 179 (4), 445-461.
43. Kamusoko, C., Aniya, M., Adi, B., Manjoro, M. (2009). Rural sustainability under threat in Zimbabwe-Simulation of future land use/cover changes in the Bindura district based on the Markov-cellular automata model. Appl. Geogr., 29, 435–447.
44. Li, F., Sun, Y., Li, X., Hao X, Li, W., Qian, Y., Liu, H., Sun, H. (2016). Research on the Sustainable Development of Green Space in Beijing Using the Dynamic Systems Model. Sustainability, 8(10), 965.
45. Dallimer, M., Tang, Z., Gaston, K.J., Davies, Z.G. (2016). The extent of shifts in vegetation phenology between rural and urban areas within a human-dominated region. Ecology and Evolution, 6(7), 1942-1953.
46. Zhou, W., Wang, J., Cadenasso, M.L. (2017). Effects of the spatial configuration of trees on urban heat mitigation: A comparative study. Remote Sensing of Environment, 195,1-12.
47. Ferreira, L.S., Duarte, D.H.S. (2019). Exploring the relationship between urban form, land surface temperature, and vegetation indices in a subtropical megacity. Urban Climate, 27, 105-123.

48. Grigoras, G., Urițescu, B. (2019). Land Use/Land Cover changes dynamics and their effects on Surface Urban Heat Island in Bucharest, Romania. International Journal of Applied Earth Observation and Geoinformation, 80, 115-126.
49. Taylor, L., Hochuli, D.F. (2017). Defining greenspace: Multiple uses across multiple disciplines. Landscape and Urban Planning, 158, 25-38.
50. Crutzen, P.J. (2004). New Directions: The growing urban heat and pollution "island" effect—impact on chemistry and climate. Atmospheric Environment, 38(21), 3539-3540.
51. Voogt, J.A., Oke, T.R. (2003). Thermal remote sensing of urban climates. Remote Sensing of Environment, 86(3), 370-384.
52. Kauffmann, B., Baccelli, F., Chaintreau, A., Mhatre, V., Papagiannaki, K., Diot, C. (2007). Measurement-Based Self Organization of Interfering 802.11 Wireless Access Networks, IEEE INFOCOM 2007 - 26th IEEE International Conference on Computer Communications: Anchorage, AK, USA, 1451-1459.
53. Sherafati, S., Saradjian, M.R., Rabbani, A. (2018). Assessment of Surface Urban Heat Island in Three Cities Surrounded by Different Types of Land-Cover Using Satellite Images. J Indian Soc Remote Sens, 46, 1013–1022.
54. Gohain, K.J., Mohammad, P., Goswami, A. (2021). Assessing the impact of land use land cover changes on land surface temperature over Pune city, India. Quaternary International, 575-576, 259-269.
55. Ahmed, B., Kamruzzaman, M., Zhu, X., Rahman, M.S., Choi, K. (2013). Simulating Land Cover Changes and Their Impacts on Land Surface Temperature in Dhaka, Bangladesh. Remote Sensing, 5(11), 5969-5998.
56. Wang, J., Li, S., Cui, X., Li, H., Quan, X., Wang, C., Sun, Y. (2016). Bio accessibility, sources, and health risk assessment of trace metals in urban park dust in Nanjing, Southeast China. Ecotoxicology and Environmental Safety, 128, 161-170.
57. Guha, S., Govil, H., Mukherjee, S. (2017). Dynamic analysis and ecological evaluation of urban heat islands in Raipur City, India. Journal of Applied Remote Sensing, 11(3), 036020.
58. Priyankara, P., Ranagalage, M., Dissanayake, D., Morimoto, T., Murayama, Y. (2019). Spatial Process of Surface Urban Heat Island in Rapidly Growing Seoul Metropolitan Area for Sustainable Urban Planning Using Landsat Data (1996–2017). Climate, 7(9), 110.
59. Dissanayake, D., Morimoto, T., Murayama, Y., Ranagalage, M. (2019). Impact of Landscape Structure on the Variation of Land Surface Temperature in Sub-Saharan Region: A Case Study of Addis Ababa using Landsat Data (1986–2016). Sustainability, 11(8), 2257.
60. Roy, S., Pandit, S., Eva, E.A., Bagmar, S.H., Papia, M., Banik, L., Dube, T., Rahman, F., Razi, M.A. (2020). Examining the nexus between land surface temperature and urban growth in Chattogram Metropolitan Area of Bangladesh using long-term Landsat series data. Urban Climate, 32, 100593.
61. Jana, C., Mandal, D., Shrimali, S.S., Alam, N.M., Kumar, R., Sena, D.R., Kaushal, R. (202). Assessment of urban growth effects on green space and surface temperature in Doon Valley, Uttarakhand, India. Environ Monit Assess, 192, 257.
62. Das, N., Mondal, P., Sutradhar, S., Ghosh, R. (2021). Assessment of variation of land use/land cover and its impact on land surface temperature of Asansol subdivision. The Egyptian Journal of Remote Sensing and Space Science, 24(1), 131-149.
63. Sharma, A., Sharma, D., Panda, S.K. (2022). Assessment of spatiotemporal trend of precipitation indices and meteorological drought characteristics in the Mahi River basin, India. Journal of Hydrology, 605, 127314.
64. Sha, K., Srinivasa, A., Madhu, D. (2020). In The study on variability of NDVI over Kerala using satellite observations, AIP Conference Proceedings. Melville, NY 11747: AIP Publishing LLC, 020013–020019.
65. Guha, S., Govil, H. (2020). Land surface temperature and normalized difference vegetation index relationship: a seasonal study on a tropical city. SN Appl. Sci. 2, 1661.
66. Guha, S. (2021). Dynamic seasonal analysis on LST-NDVI relationship and ecological health of Raipur City, India. Ecosystem Health and Sustainability, 7(1).

67. Feng, Y., Li, H., Tong, X., Chen, L., Liu, Y. (2018). Projection of land surface temperature considering the effects of future land change in the Taihu Lake Basin of China. Global and Planetary Change, 167, 24-34.
68. Rahman, M.T., Aldosary, A.S., Mortoja, M.G. (2017). Modeling Future Land Cover Changes and Their Effects on the Land Surface Temperatures in the Saudi Arabian Eastern Coastal City of Dammam. Land, 6(2), 36.
69. Yuan, X., Wang, W., Cui, J., Meng, F., Kurban, A., De Maeyer, P. (2017). Vegetation changes and land surface feedbacks drive shifts in local temperatures over Central Asia. Sci Rep,7, 3287.
70. Matthews, T., Lo, A. Y., Byrne, J. A. (2015). Reconceptualizing Green Infrastructure for Climate Change Adaptation: Barriers to Adoption and Drivers for Uptake by Spatial Planners. Landsc. urban Plan., 138, 155–163.
71. Jin, M., Dickinson, R.E., Vogelmann, A.M. (1996). A Comparison of CCM2–BATS Skin Temperature and Surface-Air Temperature with Satellite and Surface Observations. Journal of Climate, 10, 1505-1524.
72. Dickinson, R. E. (1994). Satellite systems and models for future climate change. In A. Henderson-Sellers (Ed.), Future Climates of the World: A Modelling Perspective (27). World Survey of Climatology, Elsevier.
73. Qin, Z., Karnieli, A. (1999). Progress in the remote sensing of land surface temperature and ground emissivity using NOAA-AVHRR data. International Journal of Remote Sensing, 20(12), 2367-2393.
74. Prata, A. J., Caselles, V., Coll, C., Sobrino, J. A., Ottlé, C. (1995). Thermal remote sensing of land surface temperature from satellites: Current status and prospects. Remote Sensing Reviews, 12(3-4), 175-224.
75. Noran, J.M., Becker, F. (1995). Terminology in thermal infrared remote sensing of natural surfaces. Agricultural and Forest Meteorology, 77 (3-4), 153-166.
76. Matsui, T., Lakshmi, V., Small, E. (2002). Links between Snow Cover, Surface Skin Temperature, and Rainfall Variability in the North American Monsoon System. Journal of Climate, 16(11), 1821-1829.
77. Pinheiro, A.C.T., Privette, J.L., Guillevic, P. (2006). Modeling the observed angular anisotropy of land surface temperature in a Savanna. IEEE Transactions on Geoscience and Remote Sensing, 44(4), 1036-1047.
78. Kimes, D. S., Idso, S. B., Pinter, P. J., Reginato, R. J., Jackson, R. D. (1980). View angle effects in the radiometric measurement of plant canopy temperature. Remote Sensing of Environment, 10, 273-284.
79. Kimes, D. S., Kirchner, J. A. (1983). Directional radiometric measurements of row-crops temperatures. International Journal of Remote Sensing, 4, 299-311.
80. Ignatov, A. M., Dergileva, I. L. (1994). Angular effect in dual-window AVHRR brightness temperatures over oceans. International Journal of Remote Sensing, 15, 3845-3850.
81. Becker, F., Li, Z.-L. (1995). Surface Temperature and Emissivity at Various Scales: Definition, Measurement and Related Problems. Remote Sensing Reviews, 12, 225 – 53.
82. Mumtaz, F., Tao, Y., De Leeuw, G., Zhao, L., Fan, C., Elnashar, A., et al. (2020). ModelingSpatio-Temporal Land Transformation and its Associated Impacts on Land Surface Temperature (LST). Remote Sens., 12, 2987.
83. Choudhury, D., Das, K., Das, A. (2019). Assessment of land use land cover changes and its impact on variations of land surface temperature in Asansol-Durgapur Development Region. The Egyptian Journal of Remote Sensing and Space Science, 22(2), 203-218.
84. Xiong, Y., Huang, S., Chen, F., Ye, H., Wang, C., Zhu, C. (2012). The Impacts of Rapid Urbanization on the Thermal Environment: A Remote Sensing Study of Guangzhou, South China. Remote Sens., 4, 2033–2056.
85. Mathew, A., Khandelwal, S., Kaul, N. (2018). Analysis of Diurnal Surface Temperature Variations for the Assessment of Surface Urban Heat Island Effect over Indian Cities. Energy Build., 159, 271–295.
86. Fu, P., Weng, Q. (2018). Variability in Annual Temperature Cycle in the Urban Areas of the United States as Revealed by MODIS Imagery. ISPRS J. Photogrammetry Remote Sens., 146, 65–73.
87. Santamouris, M. (2014). Cooling the Cities - A Review of Reflective and Green Roof Mitigation Technologies to Fight Heat Island and Improve Comfort in Urban Environments. Sol. Energy, 103, 682–703.

88. Waleed, M., Sajjad, M. (2022). Leveraging Cloud-Based Computing and Spatial Modeling Approaches for Land Surface Temperature Disparities in Response to Land Cover Change: Evidence from Pakistan. Remote Sens. Appl. Soc. Environ., 25, 100665.
89. Dilawar, A., Chen, B., Trisurat, Y., Tuankrua, V., Arshad, A., Hussain, Y., et al. (2021). Spatiotemporal Shifts in Thermal Climate in Responses to Urban Cover Changes: A-Case Analysis of Major Cities in Punjab, Pakistan. Geomatics, Nat. Hazards Risk, 12, 763–793.
90. Hassan, T., Zhang, J., Prodhan, F. A., Pangali Sharma, T. P., Bashir, B. (2021). Surface Urban Heat Islands Dynamics in Response to LULC and Vegetation across South Asia (2000-2019). Remote Sens., 13, 3177.
91. Bokaie, M., Zarkesh, M. K., Arasteh, P. D., Hosseini, A. (2016). Assessment of Urban Heat Island Based on the Relationship between Land Surface Temperature and Land Use/Land Cover in Tehran. Sustain. Cities Soc., 23, 94–104.
92. Solaimani, K., Arekhi, M., Tamartash, R., Miryaghobzadeh, M. (2010). Land Use/cover Change Detection Based on Remote Sensing Data (A Case Study; Neka Basin). Agric. Biol. J. N. Am., 1, 1148–1157.
93. Singh, P., Kikon, N., Verma, P. (2017). Impact of Land Uses Change and Urbanization on Urban Heat Island in Lucknow City, Central India. A Remote Sensing-Based Estimate. Sustain. cities Soc., 32, 100–114.
94. Xu, H., Wang, Y., Guan, H., Shi, T., Hu, X. (2019). Detecting Ecological Changes with a Remote Sensing Based Ecological Index (RSEI) Produced Time Series and Change Vector Analysis. Remote Sensing, 11(20), 2345.
95. Yuan, F., Bauer, M.E. (2007). Comparison of impervious surface area and normalized difference vegetation index as indicators of surface urban heat island effects in Landsat imagery. Remote Sensing of Environment, 106(3), 375-386.
96. Weng, Q., Lu, D., Schubring, J. (2004). Estimation of land surface temperature–vegetation abundance relationship for urban heat island studies. Remote Sensing of Environment, 89(4), 467-483.
97. Karnieli, A., Bayasgalan, M., Bayarjargal, Y., Khudulmur, S., Tucker, C.J. (2006). Comments on the use of the Vegetation Health Index in Mongolia. International Journal of Remote Sensing, 27(10), 2017-2024.
98. Nurwanda, A., Honjo, T. (2020). The prediction of city expansion and land surface temperature in Bogor City, Indonesia. Sustain Cities Soc, 52,101772.
99. Sekertekin A., Zadbagher E. (2021). Simulation of future land surface temperature distribution and evaluating surface urban heat island based on impervious surface area. Ecological Indicators, 122, 107230.
100. Tran, D.X., Pla, F., Latorre-Carmona, P., Myint, S.W., Caetano, M., Kieu, H.V. (2017). Characterizing the relationship between land use land cover change and land surface temperature. ISPRS Journal of Photogrammetry and Remote Sensing, 124, 119-132.
101. UNFCC. (2007). Physical and socio-economic trends in climate-related risks and extreme events, and their implications for sustainable development.
102. Fan, F., Wang, Y., Wang, Z. (2008). Temporal and spatial change detection (1998–2003) and predicting land use and land cover in the Core corridor of Pearl River Delta (China) by using TM and ETM+ images. Environ Monit Assess, 137, 127–147.
103. Rouse, J.W., Haas, R.H., Schell, J.A., Deering, D.W. (1973). Monitoring Vegetation Systems in the Great Plains with ERTS (Earth Resources Technology Satellite). Proceedings of 3rd Earth Resources Technology Satellite Symposium, Greenbelt, 10-14 December, SP-351, 309-317.
104. Akbar, T.A., Hassan, Q.K., Ishaq, S., Batool, M., Butt, H.J., Jabbar, H. (2019). Investigative Spatial Distribution and Modelling of Existing and Future Urban Land Changes and Its Impact on Urbanization and Economy. Remote Sensing, 11(2),105.
105. Bhandari, A.K., Kumar, A., Singh, G.K. (2012). Feature Extraction using Normalized Difference Vegetation Index (NDVI): A Case Study of Jabalpur City. Procedia Technology, 6, 612-621.
106. Xu, H. (2006). Modification of normalized difference water index (NDWI) to enhance open water features in remotely sensed imagery. International Journal of Remote Sensing, 27(14), 3025-3033.

107. Szabó, S., Enyedi, P. et al. (2016). Automated registration of potential locations for solar energy production with light detection and ranging (LiDAR) and small format photogrammetry. J Clean Prod, 112(5), 3820–3829.
108. Mukherjee, N.R., Samuel, C. (2016). Assessment of the Temporal Variations of Surface Water Bodies in and around Chennai using Landsat Imagery. Indian Journal of Science and Technology, 9(18), 1-7.
109. Zha, Y., Gao, J., Ni, S. (2003). Use of normalized difference built-up index in automatically mapping urban areas from TM imagery. International Journal of Remote Sensing, 24(3), 583-594.
110. Dhar, R.B., Chakraborty, S., Chattopadhyay, R. et al. (2019). Impact of Land-Use/Land-Cover Change on Land Surface Temperature Using Satellite Data: A Case Study of Rajarhat Block, North 24-Parganas District, West Bengal. J Indian Soc Remote Sens, 47, 331–348.
111. Rasul, A., Balzter, H., Ibrahim, G.R.F., Hameed, H.M., Wheeler, J., Adamu, B., Ibrahim, S., Najmaddin, P.M. (2018). Applying Built-Up and Bare-Soil Indices from Landsat 8 to Cities in Dry Climates. Land, 7(3), 81.
112. Xu, H. (2008). A new index for delineating built-up land features in satellite imagery. International Journal of Remote Sensing, 29(14), 4269-4276.
113. Zhou, Y., Yang, G., Wang, S., Wang, L., Wang, F., Liu, X. (2014). A new index for mapping built-up and bare land areas from Landsat-8 OLI data. Remote Sensing Letters, 5(10), 862-871.
114. Anderson, J.R., Hardy, E.E., Roach, J.T., Witmer, R.E. (1976). A Land Use and Land Cover Classification System for Use with Remote Sensor Data. Geological Survey Professional Paper No. 964, U.S. Government Printing Office, Washington DC, 28.
115. Clarke, K.C., Hoppen, S., Gaydos, L. (1997). A Self-Modifying Cellular Automaton Model of Historical Urbanization in the San Francisco Bay Area. Environment and Planning B: Urban Analytics and City Science, 24(2).
116. Wu, D., Liu, J., Wang, S. et al. (2010). Simulating urban expansion by coupling a stochastic cellular automata model and socioeconomic indicators. Stoch Environ Res Risk Assess, 24, 235–245.
117. Ottensmann, J.R. (1977). Urban Sprawl, Land Values and the Density of Development. Land Economics, 53(4), 389-400.
118. Pickett, S.T.A., Cadenasso, M.L., Grove, J.M., Nilon, C.H., Pouyat, R.V., Zipperer, W.C., Costanza, R. (2001). Urban Ecological Systems: Linking Terrestrial Ecological, Physical, and Socioeconomic Components of Metropolitan Areas. Annual Review of Ecology and Systematics, 32, 127-157.
119. Liu, J.Y., Zhan, J.Y., Deng, X.Z. (2005). Spatio-temporal Patterns and driving forces of urban land expansion in China during the economic reform era. AMBIO, 34(6), 450–455.
120. Hauser, P. M. (1966). Handbook for Social Research in Urbanization. UNESCO
121. Singh, M. (1990). Uneven development in agriculture and labor migration: a case of Bihar and Punjab. Indian Institute of Advanced Study.
122. Burgess, E.W. (1925). Residential Segregation in American Cities. The ANNALS of the American Academy of Political and Social Science, 140(1), 105-115.
123. Burgess, P. (1996). Profit, Planning, and Politics: Expanding the History of City Planning. Journal of Urban History, 22(3), 391-398.
124. Palen, J. J. (1992). The urban world (4th ed). McGraw-Hill.
125. Lewis, A. (1954). Economic development with unlimited supplies of labor. Manchester School of Economic and Social Studies, 22, 139–191.
126. Fei, J. C. H., Ranis, G. (1961). A theory of economic development. American Economic Review, 51, 533-65.
127. Todaro, M.P. (1976). Urban job expansion, induced migration, and rising unemployment: A formulation and simplified empirical test for LDCs. Journal of Development Economics, 3(3), 211-225.
128. Giri, P. (1998). Urbanization in West Bengal, 1951-1991. Economic and Political Weekly, 33.
129. World Bank. (1982). World Development Report 1982. Oxford University Press, New York.

130. Mills, E. S., Becker, C. M., Verma, S. (1986). Studies in Indian urban development. Oxford University Press.
131. Town and Country Planning Organisation. (2001). Area, Population, and Density of Cities and Towns of India – 2001. Socio-economic and Monitoring Division, Ministry of Urban Development, Government of India.
132. Katz, P., Scully, V.J., Bressi, T.W. (1994). The new urbanism: Toward an architecture of community (Vol. 10). McGraw-Hill.
133. Hoyt, H. (1966). Growth and Structure of Twenty-One Great World Cities. Land Economics, 42(1), 53–64.
134. Guohua, H., Tang, G., Li, X. (2007). Socio-economic driving forces of land-use change in Kunshan, the Yangtze River Delta economic area of China. Journal of Environmental Management, 83, 351–364.
135. Fagan, W.F., Meir, E., Carroll, S.S., Wu, J. (2001). The ecology of urban landscapes: Modeling housing starts as a density-dependent colonization process. Landscape Ecology, 16, 33-39.
136. Sinclair, R. (1967). Von Thünen and Urban Sprawl. Annals of the Association of American Geographers, 57(1), 72-87.
137. Brueckner, J.K., Fansler, D. (1983). The economics of urban sprawl: Theory and evidence on the spatial sizes of cities. Review of Economics and Statistics, 55, 479-482.
138. Lowry, I.S. (1988). Planning for Urban Sprawl. Transportation Research Board Special Report No. 220, 275–312.
139. Marzluff, J. M., Boone, R. B., Cox, G. W. (1994). Native pest bird species in the West: why have they succeeded where so many have failed? Studies Avian Biol., 15, 202–220.
140. Ewing, R.H. (2008). Characteristics, Causes, and Effects of Sprawl: A Literature Review. In Marzluff, J.M., et al. (Eds.), Urban Ecology (Springer, New York). 519-535.
141. Peiser, R.B. (1984). Does It Pay to Plan Suburban Growth? Journal of the American Planning Association, 50(4), 419-433.
142. Koenig, J. (1989). Should We Halt Urban Sprawl? Florida Trend, 31(12), 28–31.
143. Bhatta, B., Saraswati, S., Bandyopadhyay, D. (2010). Urban sprawl measurement from remote sensing data. Applied Geography, 30(4), 731-740.
144. Marathe, E. V. (2001). Modern City Form and The Problem of Urban Sprawl. Ecological and Environmental Advisory Committee 1998-2001, The Regional Municipality of Niagara.
145. Rahman, M.T. (2016). Land Use and Land Cover Changes and Urban Sprawl in Riyadh, Saudi Arabia: An Analysis Using Multi-Temporal Landsat Data and Shannon's Entropy Index. ISPRS—International Archives of the Photogrammetry, Remote Sensing and Spatial Information Sciences, 1017-1021.
146. Li., X., Zhou, W., Ouyang, Z. (2013). Forty Years of Urban Expansion in Beijing: What Is the Relative Importance of Physical, Socioeconomic, and Neighborhood Factors? Applied Geography, 38, 1-10.
147. Dewan, A.M., Yamaguchi, Y. (2009). Land Use and Land Cover Change in Greater Dhaka, Bangladesh: Using Remote Sensing to Promote Sustainable Urbanization. Applied Geography, 29, 390-401.
148. Rimal, B., Baral, H., Stork, N. E., Paudyal, K., Rijal, S. (2015). Growing City and Rapid Land Use Transition: Assessing Multiple Hazards and Risks in the Pokhara Valley, Nepal. Land, 4 (4), 957-978.
149. Rimal, B., Zhang, L., Keshtkar, H., Wang, N., Lin, Y. (2017). Monitoring and Modeling of Spatiotemporal Urban Expansion and Land-Use/Land-Cover Change Using Integrated Markov Chain Cellular Automata Model. ISPRS International Journal of Geo-Information, 6(9), 288.
150. Rimal, B. (2012). Urbanization and the Decline of Agricultural Land in Pokhara Sub- Sub-Sub-Sub-Metropolitan City, Nepal. Journal of Agricultural Science, 5, 54-65.
151. Thapa, R.B., Murayama, Y. (2010). Drivers of urban growth in the Kathmandu valley, Nepal: Examining the efficacy of the analytic hierarchy process. Applied Geography, 30(1), 70-83.
152. Rimal, B., Zhang, L., Fu, D., Kunwar, R., Zhai, Y. (2017). Monitoring Urban Growth and the Nepal Earthquake 2015 for Sustainability of Kathmandu Valley, Nepal. Land, 6(2), 42.

153. Wang, H., Liu, D., Lin, H., Montenegro, A., Zhu, X. (2015). NDVI and vegetation phenology dynamics under the influence of sunshine duration on the Tibetan plateau. International Journal of Climatology, 35(5), 687-698.
154. Sobrino, J.A., Jiménez-Muñoz, J.C., Paolini, L. (2004). Land surface temperature retrieval from LANDSAT TM 5. Remote Sensing of Environment, 90(4), 434-440.
155. Srivastava, P.K., Majumdar, T.J., Bhattacharya, A.K. (2009). Surface temperature estimation in Singhbhum Shear Zone of India using Landsat-7 ETM+ thermal infrared data. Advances in Space Research, 43(10), 1563-1574.
156. Gillespie, A. R. (1985). Lithologic mapping of silicate rocks using TIMS. In TIMS Data Users' Workshop, June 18–19, Jet Propulsion Laboratory Publication 86–38. Pasadena, CA. Jet Propulsion Lab, 29–44.
157. Li, X., Strahler, A.H., Friedl, M.A. (1999). A conceptual model for effective directional emissivity from nonisothermal surfaces. IEEE Transactions on Geoscience and Remote Sensing, 37(5), 2508-2517.
158. Li, Z., Wu, H., Wang, N. et al. (2013). Land surface emissivity retrieval from satellite data. International Journal of Remote Sensing, 34(9-10), 3084-3127.
159. Zhang, R., Tian, J., Su, H., Sun, X., Chen, S., Xia, J. (2008). Two Improvements of an Operational Two-Layer Model for Terrestrial Surface Heat Flux Retrieval. Sensors, 8(10), 6165-6187.
160. Zhang, S., Zhao, J., Frey, K., Su, J. (2013). Dual-polarized ratio algorithm for retrieving Arctic Sea ice concentration from passive microwave brightness temperature. J. Oceanogr., 69, 215–227.
161. NOAA National Centers for Environmental Information. (2017). Monthly Global Climate Report for Annual 2017. The USA.
162. Pacione, M. (2003). Urban environmental quality and human wellbeing—a social geographical perspective. Landscape and Urban Planning, 65(1-2), 19-30.
163. Rinner, C., Hussain, M. (2011). Toronto's Urban Heat Island Exploring the Relationship between Land Use and Surface Temperature. Remote Sensing, 3, 1251–1265.
164. Chen, J., Chen, J., Liao, A., et al. (2015). Global land cover mapping at 30 m resolution: A POK-based operational approach. ISPRS Journal of Photogrammetry and Remote Sensing, 103, 7-27.
165. Lo, C.P., Quattrochi, D. (2003). Land-Use and Land-Cover Change, Urban Heat Island Phenomenon, and Health Implications: A Remote Sensing Approach. Photogrammetric Engineering & Remote Sensing, 69(9),1053-1063.
166. Xiong, Q., Chen, W., He, L., Luo, S., Li, H. (2022). Study on the influencing factors and the spatiotemporal heterogeneity of Urban Heat Island effect in Nanchang City of China. J. Asian Arch. Build. Eng., 22, 1444–1457.
167. Weng, X.P., Yang, X.F. (2011). Urban Heat Island Monitoring and Analysis Using Landsat ETM+/TM Imageries. Key Eng. Mater., 3–6, 467–469.
168. Xiao, R., Ouyang, Z., Zhang, Z., Wang, X., Li, W., Zheng, H. (2005). Advances in Methodology of Urban Heat Island. Meteorol. Mon, 11, 4–7.
169. Grover, A., Singh, R.B. (2015). Analysis of Urban Heat Island (UHI) about Normalized Difference Vegetation Index (NDVI): A Comparative Study of Delhi and Mumbai. Environments, 2(2), 125-138.
170. Appiah, D. O., Forkuo, E. K., Bugri, J. T. (2015). Land use conversion probabilities in a peri-urban district of Ghana. Chin. J. Urban Environ. Stud., 3, 1550026.
171. Sohail, M. T., Mahfooz, Y., Azam, K., Yen, Y., Genfu, L., Fahad, S. (2019). Impacts of urbanization and land cover dynamics on underground water in Islamabad, Pakistan. DESALINATION WATER Treat., 159, 402–411.
172. Nguyen, T. T., Barber, P., Harper, R., Linh, T. V. K., Dell, B. (2020). Vegetation trends associated with urban development: The role of golf courses. PLoS one, 15, e0228090.
173. Liu, Y., Shaker Ul, D., Jiang, Y. (2021). Urban growth sustainability of Islamabad, Pakistan, over the last 3 decades: A perspective based on object-based backdating change detection. GeoJournal, 86, 2035–2055.

174. Sahani, N. (2021). Assessment of spatio-temporal changes of land surface temperature (LST) in Kanchenjunga Biosphere Reserve (KBR), India using Landsat satellite image and single-channel algorithm. Remote Sens. Appl. Soc. Environ., 24, 100659.
175. Deng, Y., Wang, S., Bai, X., Tian, Y., Wu, L., Xiao, J., et al. (2018). Relationship among land surface temperature and LUCC, NDVI in typical karst area. Sci. Rep., 8, 1–12.
176. Li, W., Cao, Q., Lang, K., Wu, J. (2017). Linking potential heat source and sink to urban heat island: Heterogeneous effects of landscape pattern on land surface temperature. Science of The Total Environment, 586, 457-465.
177. Guha, S., Govil, H., Dey, A., Gill, N. (2020). A case study on the relationship between land surface temperature and land surface indices in Raipur City, India. GeogrTidsskr., 120(1), 35–50.
178. McFeeters, S.K. (1996). The use of the Normalized Difference Water Index (NDWI) in the delineation of open water features. International Journal of Remote Sensing, 17(7), 1425-1432.
179. Chen, X., Zhao, H., Li, P., Yin, Z. (2006). Remote sensing image-based analysis of the relationship between urban heat island and land use/cover changes. Remote Sensing of Environment, 104(2), 133-146.
180. Essa, W., Verbeiran, B., van der Kwast, J., et al. (2012). Evaluation of the DisTrad thermal sharpening methodology for urban areas. International Journal of Applied Earth Observation and Geoinformation, 19, 163-172.
181. Yuan, X., Longhui, L., Xi, C., Hao, S. (2015). Effects of precipitation intensity and temperature on NDVI-based grass change over Northern China during the period from 1982 to 2011. Remote Sensing, 7(8), 10164–10183.
182. Ghobadi, Y., Pradhan, B., Shafri, H.Z.M., Kabiri, K. (2014). Assessment of the spatial relationship between land surface temperature and land use/cover retrieval from multi-temporal remote sensing data in South Karkheh Sub-basin, Iran. Arab J Geosci., 8(1), 525–537.
183. Wu, C., Li, J., Wang, C., Song, C., Chen, Y., Finka, M., Rosa, D.L. (2019). Understanding the relationship between urban blue infrastructure and land surface temperature. Sci Total Environ., 694, 133742.
184. Zhang, X., Estoque, R.C., Murayama, Y. (2017). An urban heat island study in Nanchang City, China based on land surface temperature and social-ecological variables. Sustain Cities Soc., 32, 557–568.
185. Weng, Q. (2001). A remote sensing-GIS evaluation of urban expansion and its impact on surface temperature in the Zhujiang Delta, China. Int J Remote Sens, 22(10),1999–2014.
186. Xiao, H., Weng, Q. (2007). The Impact of Land Use and Land Cover Changes on Land Surface Temperature in a Karst Area of China. Journal of Environmental Management, 85, 245-257.
187. Ren, C., Lau, K.L., Yiu, K., Ng, E. (2013). The application of urban climatic mapping to the urban planning of high-density cities: The case of Kaohsiung, Taiwan. Cities, 31, 1-16.
188. Feyisa, G.L., Meilby, H., Jenerette, G.D., Pauliet, S. (2016). Locally optimized separability enhancement indices for urban land cover mapping: Exploring thermal environmental consequences of rapid urbanization in Addis Ababa, Ethiopia. Remote Sensing of Environment, 175, 14-31.
189. Lopez, J.M.R, Heider, K., Scheffran, J. (2017). Frontiers of urbanization: Identifying and explaining urbanization hot spots in the south of Mexico City using human and remote sensing. Applied Geography, 79, 1-10.
190. Pearsall, H. (2017). Staying cool in the compact city: Vacant land and urban heating in Philadelphia, Pennsylvania. Applied Geography, 79, 84-92.
191. Maithani, S., Nautiyal, G., Sharma, A. (2020). Investigating the Effect of Lockdown During COVID-19 on Land Surface Temperature: Study of Dehradun City, India. J Indian Soc Remote Sens, 48, 1297–1311.
192. Cobbinah, P.B., Amoako, C. (2012). Urban Sprawl and the Loss of Peri-Urban Land in Kumasi, Ghana. International Journal of Social and Human Sciences, 6, 388-397.
193. Sharma, R., Joshi, P.K. (2013). Monitoring Urban Landscape Dynamics over Delhi (India) Using Remote Sensing (1998-2011) Inputs. Journal of Indian Society of Remote Sensing, 41, 641-650.

194. Maithani, S. (2009). A neural network-based urban growth model of an Indian city. J Indian Soc Remote Sens, 37, 363–376.
195. Kumar, A., Pandey, A.C. (2016). Geoinformatics based groundwater potential assessment in hard rock terrain of Ranchi urban environment, Jharkhand state (India) using MCDM–AHP techniques. Groundwater for Sustainable Development, 2-3, 27-41.
196. Pawe, C.K., Saikia, A. (2017). Unplanned urban growth: land use/land cover change in the Guwahati Metropolitan Area, India. GeografiskTidsskrift-Danish Journal of Geography, 118(1), 88-100.
197. Kar, R., Reddy, G.P.O., Kumar, N., Singh, S.K. (2018). Monitoring spatio-temporal dynamics of urban and peri-urban landscape using remote sensing and GIS – A case study from Central India. The Egyptian Journal of Remote Sensing and Space Science, 21(3), 401-411.
198. Sen, S., Bhattacharjee, S. (2021). An Overview of problems due to rapid urbanization in Panihati Municipal Area: an approach through Geospatial process and Weighted Score Technique. IOSR Journal of Humanities and Social Science, 26(4), 1-10.
199. Macarof, P., Florian, S. (2017). Comparison of NDBI and NDVI as Indicators of Surface Urban Heat Island Effect in Landsat 8 Imagery: A Case Study of Iasi. Present Environment and Sustainable Development, 11(2), 141-150.
200. Howard, L. (1833). The Climate of London. IAUC
201. Ohashi, Y., Kida, H. (2002). Local Circulations Developed in the Vicinity of Both Coastal and Inland Urban Areas: A Numerical Study with a Mesoscale Atmospheric Model. J. Appl. Meteor., 41, 30-45.
202. Souch, C., Grimmond, S. (2006). Applied climatology: Urban climate. Progress in Physical Geography Earth and Environment, 30, 270-279.
203. Shirazi, S.A., Kazmi, S.J. (2014). Analysis of Population Growth and Urban Development in Lahore-Pakistan using Geospatial Techniques: Suggesting some future Options. South Asian Studies, 29(1), 269-280.
204. Bongaarts, J. (2006). The causes of stalling fertility transitions. Stud Fam Plann., 37(1), 1-16.
205. Cai, Y., Zhang, H., Zheng, P. et al. (2016). Quantifying the Impact of Land Use/Land Cover Changes on the Urban Heat Island: A Case Study of the Natural Wetlands Distribution Area of Fuzhou City, China. Wetlands, 36, 285–298.